INVERSE SOURCE PROBLEMS FOR ELLIPTIC AND PARABOLIC EQUATIONS

by

Qitong Li

A dissertation submitted to the faculty of
The University of North Carolina at Charlotte
in partial fulfillment of the requirements
for the degree of Doctor of Philosophy in
Applied Mathematics

Charlotte

2019

Approved by:

_____

Dr. Loc Nguyen

_____

Dr. Shaozhong Deng

_____

Dr. Michael Klibanov

_____

Dr. Hwan-Chyang Lin

ABSTRACT

QITONG LI. Inverse source problems for elliptic and parabolic equations. (Under the direction of DR. LOC NGUYEN)

In this dissertation, we solve two inverse problems. The first one is the inverse source problem for the Helmholtz equation that governs the wave propagating in anisotropic media. The second one is to recover the initial condition for parabolic equations from the lateral Cauchy data.

Regarding to the first problem, we propose a numerical method to compute a source function from the external measurement of the wave field generated by that source. We derive an equation which is independent of the unknown source. However, this equation is not a standard partial differential equation. A method to solve it is not yet available. By truncating the Fourier series of the wave field with respect to a special basis, we can approximate that equation by a system of elliptic partial differential equations. The solution to this "approximate" system directly yields the desired source function. We solve that system of elliptic equations by the quasi-reversibility method. The convergence of this method is proved in this dissertation via a new Carleman estimate.

Regarding to the second problem, we find the initial condition for parabolic equations from the Cauchy lateral data of their solutions. We employ a technique similar to the one mentioned in the previous paragraph. We split our method into two stages. In the first stage, we establish an additional equation for the solution to the parabolic equation. Solving this equation is challenging. The theory to solve it is not yet available. Hence, in the second stage, we approximate this equation by an elliptic system. This system is solved by the quasi-reversibility method. The convergence of the quasi-reversibility method as the measurement noise goes to zero is proved. We present the implementation of our algorithm in details and verify our method by

showing some numerical examples.

The convergence of the quasi-reversibility method in both problems are proved using Carlerman estimates. These estimates are discussed in this dissertation.

ACKNOWLEDGEMENTS

I would like to express my sincere gratitude to my advisor Dr. Loc Nguyen. I'm not able to get here without his assistance, guidance and patience.

I would also like to thank Dr. Michael Klibanov for his advices and fruitful discussions. Many thanks to Dr. Shaozhong Deng and Dr. Hwan Lin for their valuable contributions and comments on my dissertation. I also acknowledge the Mathematics and Statistics Department which gives me the opportunity to study here and supports me over the years.

Thanks my parents to encourage and support me to move toward my goal throughout my life.

TABLE OF CONTENTS

CHAPTER 1: INTRODUCTION

This dissertation aims to solve two inverse problems. The first one is to reconstruct a source term from the bondary measurement of the wave field, governed by the Helmholtz equation. The second one is to recover the initial condition for parabolic equations from the lateral Cauchy data. These two inverse problems have great real world applications in electroencephalography, biomedical imaging, brain imagine, photoacoustic tomography, seismic imaging, determine the spatially distributed temperature, and identify the pollution on the surface of rivers or lakes, and etc. [1–5]

In the first problem, we propose a numerical method to solve an inverse source problem for the Helmholtz equation in the multi-frequency regime. This is the problem of determining the unknown source from external measurement of the wave field. Some similar inverse source problems for Helmholtz-like PDEs were studied both analytically and numerically in [1, 6]. In particular, in works [6, 7] uniqueness and stability results were proven for a special case and it was also shown that the stability estimate improves when the frequency grows. The uniqueness of this inverse source problem was proven in [8] for non constant coefficients. To the best of our knowledge, past numerical methods for these problems are based on various methods of the minimization of mismatched least squares functionals. Good quality numerical solutions are obtained in [2, 8, 9] for high frequencies. However, convergence rates of minimizers to the exact solution when the noise in the data tends to zero were not studied in those papers. On the other hand, we refer here to the work [10], in which a non-iterative method, based on a fresh idea, was proposed to solve the inverse source problem for a homogenous medium. Uniqueness and stability results were proven in [10] and good quality numerical results were presented. In this dissertation we

solve the inverse source problem for inhomogeneous media. We introduce a new numerical method based on the Quasi-Reversibility Method (QRM). The Lipschitz-like convergence rate of the solution due to QRM to the exact solution, as long as the noise in the data tends to zero, is proved.

The second inverse problem is a problem of recovering the initial condition of the parabolic equation from the lateral Cauchy data. This problem has many real-world applications ; for e.g., determine the spatially distributed temperature inside a solid from the boundary measurement of the heat and heat flux in the time domain [11]; identify the pollution on the surface of the rivers or lakes [12]; effectively monitor the heat conductive processes in steel industries, glass and polymer forming and nuclear power station [13]. Due to its realistic applications, this problem has been studied intensively. The uniqueness of such similar problems is well-known, see [14]. Also, it can be reduced from the logarithmic stability results in [11,13]. The natural approach to solve this problem is the optimal control method; that means, minimize a mismatch functional. The proof of the convergence of the optimal control method to the true solution to these inverse problems is challenging and is omitted. In this dissertation, we introduce an approximate model, as a coupled linear system of elliptic partial differential equations. Solution to this model is the vector of Fourier coefficients of the solutions to the parabolic equation mentioned above. This approximate model is solved by the quasi-reversibility method. We will prove the convergence for the quasi-reversibility method as the measurement noise tends to 0. The convergent rate is Lipschitz. We present the implementation of our algorithm in details and verify our method by showing some numerical examples. More details can be found in section 1.2.

1.1 The problem of reconstructing the source terms

Below $\mathbf{x} = (x_1, ..., x_{n-1}, z) \in \mathbb{R}^n$, $n \geq 2$. Let Ω be the cube $(-R, R)^n \subset \mathbb{R}^n$ for some $R \geq 1$, and

$$\Gamma_+ = \{\mathbf{x} \in \partial\Omega : z = R\}. \tag{1.1.1}$$

For $i, j = 1, ..., n$, let functions $a_{ij} \in C^1(\mathbb{R}^n), b_j \in C(\mathbb{R}^n), c \in C(\mathbb{R}^n)$ be such that:

1. For all $\mathbf{x} \in \mathbb{R}^n$

$$a_{ij}(\mathbf{x}) = a_{ji}(\mathbf{x}) \quad 1 \leq i, j \leq n. \tag{1.1.2}$$

2. There exist two constants μ_1 and μ_2 such that $0 < \mu_1 \leq \mu_2$ and

$$\mu_1|\xi|^2 \leq \sum_{i,j=1}^{n} a_{ij}(\mathbf{x})\,\xi_i\xi_j \leq \mu_2|\xi|^2 \quad \text{for all } \mathbf{x} \in \mathbb{R}^n, \xi \in \mathbb{R}^n. \tag{1.1.3}$$

3. For all $\mathbf{x} \in \mathbb{R}^n \setminus \Omega$

$$a_{ij}(\mathbf{x}) = \begin{cases} 1 & \text{if } i = j, \\ 0 & \text{if } i \neq j. \end{cases} \tag{1.1.4}$$

4. For all $\mathbf{x} \in \mathbb{R}^n \setminus \Omega$,

$$b_j(\mathbf{x}) = c(\mathbf{x}) = 0. \tag{1.1.5}$$

We introduce the uniformly elliptic operator

$$Lu = \sum_{i,j=1}^{n} a_{ij}(\mathbf{x})u_{x_ix_j} + \sum_{i=1}^{n} b_i(\mathbf{x})u_{x_i} + c(\mathbf{x})u \quad \text{for } u \in H^2(\mathbb{R}^n). \tag{1.1.6}$$

The principal part of this operator is

$$L_0u = \sum_{i,j=1}^{n} a_{ij}(\mathbf{x})u_{x_ix_j}. \tag{1.1.7}$$

Let $k > 0$ be the wave number and $u = u(\mathbf{x}, k)$ be the complex valued wave field

of wave number k, generated by the source function which has the form of separable variables $g(k)f(\mathbf{x})$, where functions $g \in C^1[0,\infty)$ and $f \in C^1(\mathbb{R}^n)$. The wave field $u(\mathbf{x},k) \in C^2(\mathbb{R}^n), k > 0$, satisfies the equation

$$Lu + k^2\mathbf{n}^2(\mathbf{x})u(\mathbf{x},k) = g(k)f(\mathbf{x}), \quad \mathbf{x} \in \mathbb{R}^n \tag{1.1.8}$$

and the Sommerfeld radiation condition

$$\partial_{|\mathbf{x}|}u(\mathbf{x},k) - \mathrm{i}ku(\mathbf{x},k) = o(|\mathbf{x}|^{(1-n)/2}), \quad |\mathbf{x}| \to \infty. \tag{1.1.9}$$

Here, the function $\mathbf{n} \in C^1(\mathbb{R}^n)$ is the spatially distributed refractive index. We assume that

$$\mathbf{n}(\mathbf{x}) = 1 \qquad \text{for } \mathbf{x} \in \mathbb{R}^n \setminus \Omega. \tag{1.1.10}$$

Condition (1.1.10) means that the refractive index of the background (air or vacuum) is scaled to be 1. See [15] for the well-posedness of problem (1.1.8)–(1.1.9) in the case $L = \Delta$. The well-posedness for the general operator L is an assumption in this dissertation. Given numbers $\underline{k}$ and $\overline{k}$ such that $0 < \underline{k} < \overline{k} < \infty$ and assuming that the function

$$g : [\underline{k}, \overline{k}] \to \mathbb{R}$$

is known, we are interested in the following problem.

Problem 1 (Inverse source problem with Cauchy data)**.** *Reconstruct the functions $f(\mathbf{x})$, $\mathbf{x} \in \Omega$, given the following data*

$$F(\mathbf{x},k) = u(\mathbf{x},k) \quad \mathbf{x} \in \partial\Omega, k \in (\underline{k}, \overline{k}) \tag{1.1.11}$$

and

$$G(\mathbf{x},k) = \partial_\nu u(\mathbf{x},k) \quad \mathbf{x} \in \Gamma_+, k \in (\underline{k}, \overline{k}) \tag{1.1.12}$$

where u is the solution of (1.1.8),(1.1.9).

Problem 1 is somewhat over-determined due to the additional data $G(\mathbf{x},k)$ measured on $\Gamma_+ \times [\underline{k},\overline{k}]$. We need this data for the convergence theorem. However, we notice in our numerical experiments that our method works well without that additional data. More precisely, in addition to Problem 1, we also solve the following non-overdetermined problem.

Problem 2 (Inverse source problem with Dirichlet data)**.** *Reconstruct the functions $f(\mathbf{x})$, $\mathbf{x} \in \Omega$, given the following data*

$$F(\mathbf{x},k) = u(\mathbf{x},k) \quad \mathbf{x} \in \partial\Omega, k \in (\underline{k},\overline{k}) \tag{1.1.13}$$

where u is the solution of (1.1.8),(1.1.9).

The Dirichlet boundary data (1.1.13) implicitly contain the Neumann boundary data for the function u on the entire boundary $\partial\Omega$. Indeed, for each $k \in (\underline{k},\overline{k})$ one can uniquely solve equation (1.1.8) with the radiation condition (1.1.9) and boundary condition (1.1.13) in the unbounded domain $\mathbb{R}^n \setminus \Omega$. The resulting solution provides the Neumann boundary condition $\partial_\nu u(\mathbf{x},k)$ for $\mathbf{x} \in \partial\Omega, k \in (\underline{k},\overline{k})$, where ν is the unit outward normal vector at $\partial\Omega$.

We propose a new numerical method which enables us to establish convergence rate of minimizers of a certain functional of the Quasi-Reversibility Method (QRM) to the exact solution, as long as the noise in the data tends to zero. Our method is based on several ingredients:

1. Elimination of the unknown source function $f(\mathbf{x})$ from the original PDE via the differentiation with respect to k of the function $u(\mathbf{x},k)/g(k)$.

2. The use of a newly published orthonormal basis in $L^2\left(\underline{k},\overline{k}\right)$, see [16], to obtain an overdetermined boundary value problem for a system of coupled elliptic

PDEs of the second order.

3. The use of the QRM to find an approximate solution of that boundary value problem.

4. The formulation and the proof of a new Carleman estimate for the operator L_0 in (1.1.7).

5. In the case of Problem 1, the use of this Carleman estimate for establishing the convergence rate of the minimizers of the QRM to the exact solution, as long as the noise in the data tends to zero.

Recently a similar idea was applied to develop a new numerical method for the X-ray computed tomography with a special case of incomplete data [17] as well as to the development of a globally convergent numerical method for a 1D coefficient inverse problem [18]. The above items 1, 4 and 5 have roots in the Bukhgeim-Klibanov method, which was originally introduced in [19]. Even though there exists now a significant number of publications on this method, we refer here only to a few of them [20–23] since this thesis is not about that method. The original goal of [19] was to prove uniqueness theorems for coefficient inverse problems. Nowadays, however, ideas of this method are applied for constructions of numerical methods for coefficient inverse problems and other ill-posed problems, see, e.g. [16, 18, 24, 25].

Given $N > 1$, we approximate the wave field by its N^{th} partial sum of the Fourier series with respect to a special orthonormal basis. Consider the Fourier coefficients of the wave field as new unknowns. We can derive from the partial differential equation mentioned in the previous paragraph a system for such Fourier coefficients. Our numerical reconstruction is now based on a numerical solver for this system. Since this "cut-off" step is not rigorous, the obtained system is just an "approximate", rather than exact, model. However, we still employ this technique since it is quite efficient in solving many linear and nonlinear inverse problems [17, 18, 24–28].

Note that the system for Problem 1 is over-determined since the boundary data involves both Dirichlet and Neumann information of the wave field. The over-determined boundary value problem for the system of PDEs for Problem 1 by the quasi-reversibility method. This method is well-known to be a perfect tool to solve overdetermined boundary value problems for PDEs. The quasi-reversibility method was first introduced by Lattès and Lions [29] for numerical solutions of ill-posed problems for PDEs. It has been studied intensively since then, see e.g., [23, 30–36].

A survey on this method can be found in [37]. The solutions of the systems above due to the quasi-reversibility method are called the regularized solutions. The convergence of the regularized solutions to the true ones as the noise tends to 0 was proved in [24] using Carleman estimates for the case when $L = \Delta$ for spherical domains. In this thesis, we extend the Carleman estimate for the case M is not necessarily identical to Id and then use it to prove the convergence of the quasi-reversibility method. In contrast, the well-posedness for Problem 2 is only studied numerically in this dissertation.

We will prove a Carleman estimate in Section 2.2.1. We introduce the algorithms and the quasi-reversibility method to solve Problems 1 and 2 in Section 3.1. In Section 3.3, we discuss about the convergence of the regularized solutions. Then, in Section 3.4, we describe the implementation leading to the numerical results and show several numerical examples.

1.2 The problem to the parabolic equation

Let $d \geq 2$ be the spatial dimension and Ω be a open and bounded domain in $\mathbb{R}^d$. Assume that $\partial\Omega$ is smooth. Let

$$A = (a_{ij})_{i,j=1}^{d} \in C^2(\mathbb{R}^d, \mathbb{R}^{d\times d}) \tag{1.2.1}$$

satisfy the following conditions

1. A is symmetric; i.e, $A^T(\mathbf{x}) = A(\mathbf{x})$ for all $\mathbf{x} \in \mathbb{R}^d$;

2. A is uniformly elliptic; i.e., there exists a positive number μ such that

$$A(\mathbf{x})\xi \cdot \xi \geq \mu|\xi|^2 \quad \text{for all } \mathbf{x}, \xi = (\xi_1, \ldots, \xi_d) \in \mathbb{R}^d. \tag{1.2.2}$$

Let $\mathbf{b} = (b_1, b_2, \ldots, b_d) \in C^1(\mathbb{R}^d, \mathbb{R}^d)$ and $c \in C^1(\mathbb{R}^d, \mathbb{R})$. Employ the operator L (1.1.6) defined in the previous section, we have

$$Lv = \sum_{i,j=1}^{n} a_{ij}(\mathbf{x}) v_{x_i x_j} + \sum_{i=1}^{n} b_i(\mathbf{x}) v_{x_i} + c(\mathbf{x}) v \quad \text{for } v \in C^2(\mathbb{R}^d). \tag{1.2.3}$$

Consider the initial value problem

$$\begin{cases} u_t(\mathbf{x}, t) &= Lu(\mathbf{x}, t) \quad \mathbf{x} \in \mathbb{R}^d, t > 0 \\ u(\mathbf{x}, 0) &= f(\mathbf{x}) \qquad \mathbf{x} \in \mathbb{R}^d \end{cases} \tag{1.2.4}$$

where $f \in L^2(\mathbb{R}^d)$ represents an initial source with support compactly contained in Ω. We refer the reader to the books [38,39]. The second main aim of this dissertation is to solve the following problem.

Problem 3. *Let $T > 0$. Given the lateral Cauchy boundary data*

$$F(\mathbf{x}, t) = u(\mathbf{x}, t) \quad \textit{and} \quad G(\mathbf{x}, t) = \partial_\nu u(\mathbf{x}, t) \tag{1.2.5}$$

for $\mathbf{x} \in \partial\Omega, t \in [0, T]$, determine the function $f(\mathbf{x})$, $\mathbf{x} \in \Omega$.

Problem 3 is the problem of recovering the initial condition of the parabolic equation from the lateral Cauchy data. In this dissertation, we employ the technique developed by our own research group. The main point of this technique is to derive an approximate model for the Fourier coefficients of the solution to the governing partial differential equation. This technique was first introduced in [16]. This approximate

model is a system of elliptic equations. It, together with Cauchy boundary data, is solved by the quasi-reversibility method. This approach was used to solve an inverse source problem for Helmholtz equation [40] and to inverse the Radon transform with incomplete data [17]. Especially, Klibanov, Li and Zhang [41] used the convexification method, a stronger version of this technique, to compute numerical solutions to the nonlinear problem of electrical impedance tomography with restricted Dirichlet-to-Neumann map data. It is remarkable mentioning that the numerical solutions in [41] due to the convexification method are impressive.

As mentioned in the previous paragraph, we employ the quasi-reversibility method to solve an approximate model for Fourier coefficients of the solution to (1.2.4). This method was first introduced by Lattès and Lions [29]. It is used to computed numerical solutions to ill-posed problems for partial differential equations. Due to its strength, since then, the quasi-reversibility method attracts the great attention of the scientific community see e.g., [23, 30–35, 42–44]. We refer the reader to [37] for a survey on this method. The solution of the approximate model in the previous paragraph due to the quasi-reversibility method is called *regularized solution* in the theory of ill-posed problems [45]. A question arises immediately about the convergence of the quasi-reversibility method: whether or not the regularized solutions obtained by the quasi-reversibility method converges to the true solution of our system of partial differential equations as the noise tends to 0. The affirmative answer to this question is obtained using a general Carleman estimate. Moreover, we employ a Carleman estimate (in section 2.2.2) to prove that the convergence rate is Lipschitz. It is important mentioning that in the celebrate paper [19], Bukhgeim and Klibanov discovered the use of Carleman estimate in studying inverse problems for all three main types of partial differential equations.

CHAPTER 2: Preliminaries

2.1 An orthonormal basis in $L^2(a,b)$

For each $n > 1$, define $\phi_n(k) = (k-k_0)^{n-1}\exp(k-k_0)$, $k \in (a,b)$, where $k_0 = (a+b)/2$. The sequence $\{\phi_n\}_{n=1}^{\infty}$ is complete in $L^2(a,b)$. Using the Gram-Schmidt orthonormalization for the sequence $\{\phi_n\}_{n=1}^{\infty}$, we construct an orthonormal basis of $L^2(a,b)$, named as $\{\Psi_n\}_{n=1}^{\infty}$. For each n, the function $\Psi_n(k)$ takes the form

$$\Psi_n(k) = P_{n-1}(k-k_0)\exp(k-k_0)$$

where P_{n-1} is a polynomial of the $(n-1)^{\text{th}}$ order.

Fix a positive integer N. We approximate the function $u = u(\mathbf{x},k)$, $\mathbf{x} \in \Omega$, $k \in (\underline{k},\overline{k})$ by its N^{th} partial sum of its Fourier series

$$u(\mathbf{x},k) = \sum_{n=1}^{N} u_n(\mathbf{x})\Psi_n(k) \tag{2.1.1}$$

where

$$u_n(\mathbf{x}) = \int_a^b u(\mathbf{x},k)\Psi_n(k)dk.$$

In the truncation context (2.1.1), the partial derivative with respect to k of $u(\mathbf{x},k)$ is approximated by

$$\partial_k u(\mathbf{x},k) = \sum_{n=1}^{N} u_n(\mathbf{x})\Psi_n'(k) \tag{2.1.2}$$

for all $\mathbf{x} \in \Omega$ and $k \in (a,b)$. To reconstruct the wave field $u(\mathbf{x},k)$, we compute $u_n(\mathbf{x})$, $1 \le n \le N$, via (2.1.1), (2.1.2) and the knowledge of Ψ_n and Ψ_n'. We therefore require that the function Ψ_n' cannot be identically 0. The “sin and cosine" basis of the usual

Fourier transform does not meet this requirement while it is not hard to verify that the basis $\{\Psi_n\}_{n=1}^{\infty}$ does.

It is important to mention that the basis $\{\Psi_n\}_{n=1}^{\infty}$ was first introduced in [16]. Then, it is successfully used to solve nonlinear coefficient inverse problems [18, 24] and the inverse X-ray tomographic problem with incomplete data [17].

The following result plays an important role in our analysis.

Proposition 2.1.1 (Theorem 2.1 [16]). *For $m, r \geq 1$, we have*

$$d_{mr} = \int_{\underline{k}}^{\overline{k}} \Psi_m(k)\Psi_r'(k)dk = \begin{cases} 1 & \text{if } r = m, \\ 0 & \text{if } r < m. \end{cases} \tag{2.1.3}$$

Consequently, let $N > 1$ be an integer. Then the $N \times N$ matrix

$$D_N = (d_{mr})_{m,r=1}^{N} \tag{2.1.4}$$

has determinant 1 and is invertible.

2.2 Carleman estimates

2.2.1 A Carleman estimate for general elliptic operators

The main aim of this section is to prove the following estimate 2.2.1.

For brevity, we assume that the function u in Theorem 2.2.1 is a real valued one. Indeed, this theorem holds true for complex valued function u. This fact follows directly from the theorem itself. Hence, in this section, we define the space

$$H_{0,\#}^2(\Omega) = \left\{w \in H^2(\Omega) : w\mid_{\partial\Omega} = 0, \partial_\nu w\mid_{\Gamma_+} = 0\right\}$$

in (3.2.7) as the set of all real valued functions satisfying the same constraints. Recall the operator the uniformly elliptic operator L_0 in (1.1.7).

Theorem 2.2.1 (Carleman estimate)**.** *Let the number $b > R$. Let the coefficients $a_{ij}(\mathbf{x})$ of the uniformly elliptic operator L_0 defined in (1.1.7) satisfy conditions (1.1.2), (1.1.3) and also $a_{ij} \in C^1(\overline{\Omega})$. Suppose that*

$$a_{in}(\mathbf{x}) = 0, \quad \text{for } \mathbf{x} \in \partial\Omega \setminus \{z = \pm R\}, i \neq n. \tag{2.2.1}$$

Then there exist numbers

$$p_0 = p_0\left(\mu_1, \mu_2, b, n, R, \max_{ij} \|a_{ij}\|_{C^1(\overline{\Omega})}\right) > 1$$

and

$$\lambda_0 = \lambda_0\left(\mu_1, \mu_2, b, n, R, \max_{ij} \|a_{ij}\|_{C^1(\overline{\Omega})}\right) \geq 1,$$

both of which depend only on listed parameters, such that the following Carleman estimate holds:

$$\int_\Omega (L_0 u)^2 \exp\left[2\lambda (z+b)^p\right] d\mathbf{x} \geq C_2 \lambda \int_\Omega \left[(\nabla u)^2 + \lambda^2 u^2\right] \exp\left[2\lambda (z+b)^p\right] d\mathbf{x}, \tag{2.2.2}$$

for all $\lambda \geq \lambda_0$, $p \geq p_0$ and $u \in H^2_{0,\#}(\Omega)$. Here, the constant

$$C_2 = C_2\left(\mu_1, \mu_2, b, p, n, R, \max_{ij} \|a_{ij}\|_{C^1(\overline{\Omega})}\right) > 0$$

depends only on listed parameters.

Proof. Below in this proof $u \in C^2\left(\overline{\Omega}\right) \cap H^2_{0,\#}(\Omega)$. The case $u \in H^2_{0,\#}(\Omega)$ can be obtained via the density argument. In this proof $C_2 > 0$ denotes different positive numbers depending only on above listed parameters. On the other hand, everywhere below $C_3 = C_3\left(\mu_1, \mu_2, b, R, \max_{ij} \|a_{ij}\|_{C^1(\overline{\Omega})}\right) > 0$ also denotes different positive constants depending only on listed parameters but independent on p, unlike C_2. Also, in this proof $O(1/\lambda)$ denotes different functions belonging to $C^1\left(\overline{\Omega}\right)$ and satisfying

the estimate

$$\left\| O\left(1/\lambda\right) \right\|_{C^1(\overline{\Omega})} \leq \frac{C_2}{\lambda} \quad \text{for all } \lambda, p \geq 1. \tag{2.2.3}$$

Below $n-$D vector functions U_k are such that

$$\int_{\partial\Omega} U_r \cdot \nu d\sigma \geq 0 \quad r \in \{1, ..., 14\}, \tag{2.2.4}$$

where $U_r \cdot \nu$ means the scalar product of vectors U_r and ν in $\mathbb{R}^n$: recall that ν is the outward looking unit normal vector on $\partial\Omega$. In fact it follows from the proof that, the integrals in (2.2.4) equal zero for $r = 1, 2$. But they are non-negative starting from $r = 3$.

Introduce the new function $v\left(\mathbf{x}\right) = u\left(\mathbf{x}\right) \exp\left[\lambda\left(z+b\right)^p\right]$. Then

$$u\left(\mathbf{x}\right) = v\left(\mathbf{x}\right) \exp\left[-\lambda\left(z+b\right)^p\right].$$

Using straightforward calculations, we obtain

$$u_{x_i x_j} = v_{x_i x_j} \exp\left[-\lambda\left(z+b\right)^p\right] \quad \text{for } i, j = 1, \ldots, n-1,$$
$$u_{x_i z} = \left(v_{x_i z} - \lambda p \left(z+b\right)^{p-1} v_{x_i}\right) \exp\left[-\lambda\left(z+b\right)^p\right], \quad \text{for } i, j = 1, \ldots, n-1,$$

and

$$u_{zz} = \left(v_{zz} - 2\lambda p \left(z+b\right)^{p-1} v_z + \lambda^2 p^2 \left(z+b\right)^{2p-2} \left(1 + O\left(1/\lambda\right)\right) v\right) \exp\left[-\lambda\left(z+b\right)^p\right].$$

Hence, (1.1.7) implies that

$$(L_0u)\exp\left[\lambda(z+b)^p\right]$$
$$=\left[\left(\sum_{i,j=1}^{n-1}a_{ij}v_{x_ix_j}+\sum_{i=1}^{n-1}a_{in}v_{x_iz}+a_{nn}v_{zz}\right)+\left(\lambda^2p^2(z+b)^{2p-2}a_{nn}v\right)\right]$$
$$-2\lambda p(z+b)^{p-1}a_{nn}v_z-\lambda p(z+b)^{p-1}\sum_{i=1}^{n-1}a_{in}v_{x_i}. \quad (2.2.5)$$

Denote terms in the right hand side of (2.2.5) as y_1, y_2, y_3, y_4. More precisely,

$$y_1=\sum_{i,j=1}^{n-1}a_{ij}v_{x_ix_j}+\sum_{i=1}^{n-1}a_{in}v_{x_iz}+a_{nn}v_{zz}, \quad (2.2.6)$$

$$y_2=\lambda^2p^2(z+b)^{2p-2}a_{nn}v, \quad (2.2.7)$$

$$y_3=-2\lambda p(z+b)^{p-1}a_{nn}v_z, \quad (2.2.8)$$

$$y_4=-\lambda p(z+b)^{p-1}\sum_{i=1}^{n-1}a_{in}v_{x_i}. \quad (2.2.9)$$

It follows from (2.2.5) that

$$(L_0u)^2\exp\left[2\lambda(z+b)^p\right](z+b)^{2-p}=(y_1+y_2+y_3+y_4)^2(z+b)^{2-p}$$
$$=((y_1+y_2)+(y_3+y_4))^2(z+b)^{2-p}.$$

Thus,

$$(L_0u)^2\exp\left[2\lambda(z+b)^p\right](z+b)^{2-p}$$
$$\geq 2y_3(y_1+y_2)(z+b)^{2-p}+2y_4(y_1+y_2)(z+b)^{2-p}. \quad (2.2.10)$$

We now estimate from the below each term in the right hand side of inequality (2.2.10) separately. We do this in several steps.

Step 1. Estimate from the below of the quantity $2y_1y_3(z+b)^{2-p}$. By (2.2.6) and

(2.2.7), we have

$$
\begin{aligned}
&2y_1y_3\,(z+b)^{2-p}\\
&=-4\lambda p\,(z+b)\,a_{nn}v_z\left(\frac{1}{2}\sum_{i,j=1}^{n-1}\left(a_{ij}v_{x_ix_j}+a_{ij}v_{x_jx_i}\right)+\sum_{i=1}^{n-1}a_{in}v_{x_iz}+a_{nn}v_{zz}\right). \qquad (2.2.11)
\end{aligned}
$$

By the standard rules of the differentiation,

$$
\begin{aligned}
&-2\lambda p(z+b)a_{nn}v_z\left(a_{ij}v_{x_ix_j}+a_{ij}v_{x_jx_i}\right)\\
&\quad=-2\lambda p\left[(z+b)\,a_{nn}a_{ij}\left(v_zv_{x_i}\right)_{x_j}-(z+b)\,a_{nn}a_{ij}v_{zx_j}v_{x_i}-(z+b)\left(a_{nn}a_{ij}\right)_{x_j}v_zv_{x_i}\right]\\
&\qquad-2\lambda p\left[(z+b)\,a_{nn}a_{ij}\left(v_zv_{x_j}\right)_{x_i}-(z+b)\,a_{nn}a_{ij}v_{zx_i}v_{x_j}-(z+b)\left(a_{nn}a_{ij}\right)_{x_i}v_zv_{x_j}\right]\\
&\quad=\left[2\lambda p\,(z+b)\,a_{nn}a_{ij}v_{x_i}v_{x_j}\right]_z-2\lambda p\left((z+b)\,a_{nn}a_{ij}\right)_z v_{x_i}v_{x_j}\\
&\qquad+\left(-2\lambda p\,(z+b)\,a_{nn}a_{ij}v_zv_{x_i}\right)_{x_j}+4\lambda p\,(z+b)\left(a_{nn}a_{ij}\right)_{x_j}v_zv_{x_i}\\
&\qquad+\left(-2\lambda p\,(z+b)\,a_{nn}a_{ij}v_zv_{x_j}\right)_{x_i}+4\lambda p\,(z+b)\left(a_{nn}a_{ij}\right)_{x_i}v_zv_{x_j}.
\end{aligned}
$$

Hence,

$$
-2\lambda p\,(z+b)\,a_{nn}v_z\left(a_{ij}v_{x_ix_j}+a_{ij}v_{x_jx_i}\right)\geq-C_3\lambda p\,(\nabla v)^2+\mathrm{div}U_1, \qquad (2.2.12)
$$

see (2.2.4) for U_1.

Next, we estimate the term

$$
\begin{aligned}
&-\sum_{i=1}^{n-1}4\lambda p\,(z+b)\,a_{nn}a_{in}v_zv_{x_iz}\\
&\qquad\qquad=\sum_{i=1}^{n-1}\left(-2\lambda p\,(z+b)\,a_{nn}a_{in}v_z^2\right)_{x_i}+\sum_{i=1}^{n-1}\lambda p\,(z+b)\left(a_{nn}a_{in}\right)_{x_i}v_z^2.
\end{aligned}
$$

Hence,

$$
-\sum_{i=1}^{n-1}4\lambda p\,(z+b)\,a_{nn}a_{in}v_zv_{x_iz}\geq-C_3\lambda pv_z^2+\mathrm{div}U_2. \qquad (2.2.13)
$$

Now, $U_2 \cdot \nu = 0$ for $\mathbf{x} \in \partial\Omega$ for two reasons: first, this is because $v_z(\mathbf{x}) = 0$ for $x_i = \pm R$ and, second, due to condition (2.2.1). Hence, due to the first reason, we do not actually use here yet condition (2.2.1).

Next, we estimate the term $-4\lambda p (z+b) a_{nn}^2 v_z v_{zz}$ in (2.2.11),

$$-4\lambda p (z+b) a_{nn}^2 v_z v_{zz} = \left(-2\lambda p (z+b) a_{nn}^2 v_z^2\right)_z + 2\lambda p \left((z+b) a_{nn}^2\right)_z v_z^2. \tag{2.2.14}$$

Combining this with (2.2.11)-(2.2.14), we conclude that

$$2y_1 y_3 (z+b)^{2-p} \geq -C_3 \lambda p (\nabla v)^2 + \mathrm{div} U_3, \tag{2.2.15}$$

see (2.2.4) for U_3. Next,

$$\begin{aligned} -C_3\lambda p v_z^2 &= -C_3\lambda p \left(u_z^2 + 2\lambda p (z+b)^{p-1} u_z u + \lambda^2 p^2 (z+b)^{2p-2} u^2\right) \exp\left[2\lambda (z+b)^p\right] \\ &= -C_3\lambda p u_z^2 \exp\left[2\lambda (z+b)^p\right] - C_3\lambda^3 p^3 (z+b)^{2p-2} u^2 \exp\left[2\lambda (z+b)^p\right] \\ &\quad + \left(-C_3\lambda^2 p^2 (z+b)^{p-1} u^2 \exp\left[2\lambda (z+b)^p\right]\right)_z \\ &\quad + 2C_3\lambda^3 p^3 (z+b)^{2p-2} \left(1 + O(1/\lambda)\right) u^2 \exp\left[2\lambda (z+b)^p\right] \\ &\geq -C_3\lambda p u_z^2 \exp\left[2\lambda (z+b)^p\right] + \mathrm{div} U_4, \end{aligned} \tag{2.2.16}$$

see (2.2.4) for U_4. It follows from (2.2.12)-(2.2.16) that

$$2y_1 y_3 (z+b)^{2-p} \geq -C_3 \lambda p (\nabla u)^2 \exp\left[2\lambda (z+b)^p\right] + \mathrm{div} U_5, \tag{2.2.17}$$

see (2.2.4) for U_5.

Step 2. Estimate from the below the quantity $2y_2 y_3 (z+b)^{2-p}$. By (2.2.7) and

(2.2.8)

$$
\begin{aligned}
2y_2y_3\left(z+b\right)^{2-p} &= -4\lambda^3p^3\left(z+b\right)^{2p-1}a_{nn}^2v_zv \\
&= \left(-2\lambda^3p^3\left(z+b\right)^{2p-1}a_{nn}^2v^2\right)_z + 2\lambda^3p^3\left(2p-1\right)\left(z+b\right)^{2p-2}a_{nn}^2v^2 \\
&\qquad + 2\lambda^3p^3\left(z+b\right)^{2p-1}\left(a_{nn}^2\right)_z v^2 \\
&\geq 2\lambda^3p^3\left(2p-1\right)\left(z+b\right)^{2p-2}\mu_1^2\left(1+\frac{\left(z+b\right)\left(a_{nn}^2\right)_z}{\left(2p-1\right)\mu_1^2}\right)v^2 \\
&\qquad + \left(-2\lambda^3p^3\left(z+b\right)^{2p-1}a_{nn}^2v^2\right)_z \\
&\geq C_3\lambda^3p^4\left(z+b\right)^{2p-2}u^2\exp\left[2\lambda\left(z+b\right)^p\right] + \mathrm{div}U_6, \qquad (2.2.18)
\end{aligned}
$$

see (2.2.4) for U_6. There exists a sufficiently large number p_0,

$$
p_0 = p_0\left(\mu_1,\mu_2,b,n,R,\max_{ij}\left\|a_{ij}\right\|_{C^1\left(\overline{\Omega}\right)}\right) > 1
$$

such that

$$
1+\frac{\left(z+b\right)\left(a_{nn}^2\right)_z}{\left(2p-1\right)\mu_1^2} \geq \frac{1}{2}, \quad \text{for all } p \geq p_0. \qquad (2.2.19)
$$

Hence, (2.2.17)-(2.2.19) imply that for $p \geq p_0$

$$
\begin{aligned}
2\left(y_1+y_2\right)y_3\left(z+b\right)^{2-p} &\geq -C_3\lambda p\left(\nabla u\right)^2\exp\left[2\lambda\left(z+b\right)^p\right] \\
&\qquad + C_3\lambda^3p^4\left(z+b\right)^{2p-2}u^2\exp\left[2\lambda\left(z+b\right)^p\right] + \mathrm{div}U_7, \qquad (2.2.20)
\end{aligned}
$$

see (2.2.4) for U_7.

Step 3. Estimate $2y_1y_4\left(z+b\right)^{2-p}$, see (2.2.10); i.e., estimate

$$
\left(-2\lambda p\left(z+b\right)\sum_{k=1}^{n-1}a_{kn}v_{x_k}\right)\left(\sum_{i,j=1}^{n-1}a_{ij}v_{x_ix_j}+\sum_{i=1}^{n-1}a_{in}v_{x_iz}+a_{nn}v_{zz}\right). \qquad (2.2.21)
$$

First,

$$
\begin{aligned}
&-\lambda p\left(z+b\right)a_{kn}v_{x_k}\left(a_{ij}v_{x_ix_j}+a_{ji}v_{x_jx_i}\right)\\
&\quad=-\lambda p\left(z+b\right)a_{kn}a_{ij}\left(v_{x_k}v_{x_ix_j}+v_{x_k}v_{x_jx_i}\right)\\
&\quad=\left(-\lambda p\left(z+b\right)a_{kn}a_{ij}v_{x_k}v_{x_j}\right)_{x_i}+\lambda p\left(z+b\right)a_{kn}a_{ij}v_{x_kx_i}v_{x_j}\\
&\qquad+\lambda p\left(z+b\right)\left(a_{kn}a_{ij}\right)_{x_i}v_{x_k}v_{x_j}+\left(-\lambda p\left(z+b\right)a_{kn}a_{ij}v_{x_k}v_{x_i}\right)_{x_j}\\
&\qquad\qquad+\lambda p\left(z+b\right)a_{kn}a_{ij}v_{x_kx_j}v_{x_i}+\lambda p\left(z+b\right)\left(a_{kn}a_{ij}\right)_{x_j}v_{x_k}v_{xi}.
\end{aligned}
\tag{2.2.22}
$$

Next,

$$
\begin{aligned}
&\lambda p\left(z+b\right)a_{kn}a_{ij}v_{x_kx_i}v_{x_j}+\lambda p\left(z+b\right)a_{kn}a_{ij}v_{x_kx_j}v_{x_i}\\
&\qquad=\left(\lambda p\left(z+b\right)a_{kn}a_{ij}v_{x_i}v_{x_j}\right)_{x_k}-\lambda p\left(z+b\right)\left(a_{kn}a_{ij}\right)_{x_k}v_{x_i}v_{x_j}.
\end{aligned}
\tag{2.2.23}
$$

Hence, it follows from (2.2.22) and (2.2.23) that

$$
\left(-2\lambda p\left(z+b\right)\sum_{k=1}^{n-1}a_{kn}v_{x_k}\right)\left(\sum_{i,j=1}^{n-1}a_{ij}v_{x_ix_j}\right)\geq-C_3\lambda p\left(\nabla v\right)^2+\mathrm{div}U_8. \tag{2.2.24}
$$

Considering in (2.2.22) and (2.2.23) explicit forms of coordinates of the vector function U_8 and using (2.2.1), we conclude that U_7 satisfies condition (2.2.4).

We now estimate the term

$$
\left(-2\lambda p\left(z+b\right)\sum_{k=1}^{n-1}a_{kn}v_{x_k}\right)\left(\sum_{i=1}^{n-1}a_{in}v_{x_iz}\right). \tag{2.2.25}
$$

We have

$$
\left(-2\lambda p\left(z+b\right)\sum_{k=1}^{n-1}a_{kn}v_{x_k}\right)\left(\sum_{i=1}^{n-1}a_{in}v_{x_iz}\right)=-\lambda p\left(z+b\right)\sum_{i,k=1}^{n-1}a_{kn}a_{in}\left(v_{x_k}v_{x_iz}+v_{x_i}v_{x_kz}\right).
$$

We have:

$$-\lambda p\left(z+b\right)a_{kn}a_{in}\left(v_{x_k}v_{x_iz}+v_{x_i}v_{x_kz}\right)$$
$$=\left(-\lambda p\left(z+b\right)a_{kn}a_{in}v_{x_i}v_{x_k}\right)_z+\lambda p\left(\left(z+b\right)a_{kn}a_{in}\right)_z v_{x_i}v_{x_k}.$$

Hence, the term (2.2.25) can be estimated from the below as

$$\left(-2\lambda p\left(z+b\right)\sum_{k=1}^{n-1}a_{kn}v_{x_k}\right)\left(\sum_{i=1}^{n-1}a_{in}v_{x_iz}\right)\geq -C_3\lambda p\left(\nabla v\right)^2+\mathrm{div}U_9, \tag{2.2.26}$$

where U_9 satisfies (2.2.4).

We now estimate

$$\left(-2\lambda p\left(z+b\right)\sum_{k=1}^{n-1}a_{kn}v_{x_k}\right)a_{nn}v_{zz}. \tag{2.2.27}$$

We have

$$\begin{aligned}-2\lambda p\left(z+b\right)a_{kn}a_{nn}v_{x_k}v_{zz}&=\left(-2\lambda p\left(z+b\right)a_{kn}a_{nn}v_{x_k}v_z\right)_z+2\lambda p\left(z+b\right)a_{kn}a_{nn}v_{x_kz}v_z\\&\quad+2\lambda p\left(\left(z+b\right)a_{kn}a_{nn}\right)_z v_{x_k}v_z\\&=\left(\lambda p\left(z+b\right)a_{kn}a_{nn}v_z^2\right)_{x_k}-\lambda p\left(\left(z+b\right)a_{kn}a_{nn}\right)_{x_k}v_z^2\\&\quad+2\lambda p\left(\left(z+b\right)a_{kn}a_{nn}\right)_z v_{x_k}v_z+\left(-2\lambda p\left(z+b\right)a_{kn}a_{nn}v_{x_k}v_z\right)_z.\end{aligned}$$

Hence, the expression in (2.2.27) can be estimated as

$$\left(-2\lambda p\left(z+b\right)\sum_{k=1}^{n-1}a_{kn}v_{x_k}\right)a_{nn}v_{zz}\geq -C_3\lambda p\left(\nabla v\right)^2+\mathrm{div}U_{10}, \tag{2.2.28}$$

where (2.2.4) is valid for U_{10}. Summing up (2.2.24), (2.2.26) and (2.2.28), we obtain

$$2y_1y_4\left(z+b\right)^{2-p}\geq -C_3\lambda p\left(\nabla v\right)^2+\mathrm{div}U_{11}, \tag{2.2.29}$$

where U_{11} satisfies (2.2.4).

Step 4. Estimate $2y_2y_4\left(z+b\right)^{2-p}$,

$$2y_2y_4\left(z+b\right)^{2-p}=-2\lambda^3p^3\left(z+b\right)^{2p-1}\sum_{i=1}^{n-1}a_{in}a_{nn}v_{x_i}v$$
$$=\left(\lambda^3p^3\left(z+b\right)^{2p-1}\sum_{i=1}^{n-1}a_{in}a_{nn}v^2\right)_{x_i}+\lambda^3p^3\left(z+b\right)^{2p-1}\left(\sum_{i=1}^{n-1}\left(a_{in}a_{nn}\right)_{x_i}\right)v^2.$$

Comparing this with (2.2.10), (2.2.16), (2.2.19), (2.2.20) and (2.2.29), we obtain

$$\left(L_0u\right)^2\exp\left[2\lambda\left(z+b\right)^p\right]\left(z+b\right)^{2-p}\geq-C_3\lambda p\left(\nabla u\right)^2\exp\left[2\lambda\left(z+b\right)^p\right]$$
$$+C_3\lambda^3p^4\left(z+b\right)^{2p-2}u^2\exp\left[2\lambda\left(z+b\right)^p\right]+\mathrm{div}U_{12},\forall p\geq p_0,\quad(2.2.30)$$

where U_{12} satisfies (2.2.4).

In addition to the term $\mathrm{div}U_{12}$, the right hand side of (2.2.30) has one negative and one positive term. But,except of divergence terms (div), one must have only positive terms in the right hand side of any Carleman estimate. Therefore, we perform now Step 5.

Step 5. Estimate from the below $-\left(L_0 u\right) u \exp\left[2\lambda\left(z+b\right)^p\right]$. We have

$$
\begin{aligned}
-\left(L_0 u\right) u \exp\left[2\lambda\left(z+b\right)^p\right] &= -\sum_{i,j=1}^{n-1} a_{ij} u_{x_i x_j} u \exp\left[2\lambda\left(z+b\right)^p\right] \\
&- \sum_{i=1}^{n-1} a_{in} u_{x_i z} u \exp\left[2\lambda\left(z+b\right)^p\right] - a_{nn} u_{zz} u \exp\left[2\lambda\left(z+b\right)^p\right] \\
&= \sum_{i,j=1}^{n-1} \left(-a_{ij} u_{x_j} u \exp\left[2\lambda\left(z+b\right)^p\right]\right)_{x_i} + \sum_{i,j=1}^{n-1} a_{ij} u_{x_i} u_{x_j} \exp\left[2\lambda\left(z+b\right)^p\right] \\
&+ \sum_{i,j=1}^{n-1} \left(a_{ij}\right)_{x_i} u_{x_j} u \exp\left[2\lambda\left(z+b\right)^p\right] + \sum_{i=1}^{n-1} \left(-a_{in} u_z u \exp\left[2\lambda\left(z+b\right)^p\right]\right)_{x_i} \\
&+ \sum_{i=1}^{n-1} \left(a_{in}\right)_{x_i} u_z u \exp\left[2\lambda\left(z+b\right)^p\right] + \sum_{i=1}^{n-1} a_{in} u_z u_{x_i} \exp\left[2\lambda\left(z+b\right)^p\right] \\
&+ \left(-a_{nn} u_z u \exp\left[2\lambda\left(z+b\right)^p\right]\right)_z + a_{nn} u_z^2 \exp\left[2\lambda\left(z+b\right)^p\right] \\
&+ 2\lambda p \left(z+b\right)^{p-1} a_{nn} u_z u \exp\left[2\lambda\left(z+b\right)^p\right] + \left(a_{nn}\right)_z u_z u \exp\left[2\lambda\left(z+b\right)^p\right]. \quad (2.2.31)
\end{aligned}
$$

Next,

$$
\begin{aligned}
2\lambda p \left(z+b\right)^{p-1} a_{nn} u_z u \exp\left[2\lambda\left(z+b\right)^p\right] &= \left(\lambda p \left(z+b\right)^{p-1} a_{nn} u^2 \exp\left[2\lambda\left(z+b\right)^p\right]\right)_z \\
&- 2\lambda^2 p^2 \left(z+b\right)^{2p-2} a_{nn} u^2 \left(1+O\left(1/\lambda\right)\right) \exp\left[2\lambda\left(z+b\right)^p\right]. \quad (2.2.32)
\end{aligned}
$$

Combining (2.2.31) with (2.2.32) and taking into account (1.1.3) as well as inequalities like $u_{x_i} u \geq -u_{x_i}^2/\left(2\lambda\right) - \lambda u^2/2$, we obtain for $\lambda \geq \lambda_0$

$$
\begin{aligned}
-\left(L_0 u\right) u \exp\left[2\lambda\left(z+b\right)^p\right] &\geq \frac{\mu_1}{2} \left(\nabla u\right)^2 \exp\left[2\lambda\left(z+b\right)^p\right] \\
&- 3\lambda^2 p^2 \left(z+b\right)^{2p-2} a_{nn} u^2 \exp\left[2\lambda\left(z+b\right)^p\right] + \mathrm{div} U_{13}, \quad (2.2.33)
\end{aligned}
$$

see (2.2.4) for U_{13}.

Step 6. This is the final step. Multiply estimate (2.2.33) by $4C_3\lambda p/\mu_1$ and sum

up with (2.2.30). We obtain

$$
\begin{aligned}
&-4C_3\lambda p\mu_1^{-1}\left(L_0u\right)u\exp\left[2\lambda\left(z+b\right)^p\right]+\left(L_0u\right)^2\exp\left[2\lambda\left(z+b\right)^p\right]\left(z+b\right)^{2-p}\\
&\geq C_3\lambda p\left(\nabla u\right)^2\exp\left[2\lambda\left(z+b\right)^p\right]\\
&+C_3\lambda^3p^4\left(z+b\right)^{2p-2}\left(1-\frac{12a_{nn}}{p\mu_1}\right)u^2\exp\left[2\lambda\left(z+b\right)^p\right]+\mathrm{div}U_{14}, \quad (2.2.34)
\end{aligned}
$$

see (2.2.4) for U_{14}. We can choose p_0 so large that, in addition to (2.2.19),

$$
1-\frac{12a_{nn}\left(\mathbf{x}\right)}{p\mu_1}\geq\frac{1}{2},\forall p\geq p_0. \quad (2.2.35)
$$

We estimate the left hand side of (2.2.34) from the above as

$$
\begin{aligned}
&-4C_3\lambda p\mu_1^{-1}\left(L_0u\right)u\exp\left[2\lambda\left(z+b\right)^p\right]+\left(L_0u\right)^2\exp\left[2\lambda\left(z+b\right)^p\right]\left(z+b\right)^{2-p}\\
&\leq C_2\left(L_0u\right)^2\exp\left[2\lambda\left(z+b\right)^p\right]+C_2\lambda^2u^2\exp\left[2\lambda\left(z+b\right)^p\right].
\end{aligned}
$$

Combining this with the right hand side of (2.2.34), integrating the obtained pointwise inequality over the domain Ω and taking into account (2.2.4), (2.2.35) and Gauss' formula, we obtain the target estimate (2.2.2). □

Corollary 2.2.1. *Assume that conditions of Theorem 2.2.1 are satisfied. Since we should have in Theorem 2.2.1 $b>R$, we choose in (2.2.2) $b=3R$. Let $p_0>1$ and $\lambda_0>1$ be the numbers of Theorem 2.2.1. Consider the $N-D$ complex valued vector functions $W\left(\mathbf{x}\right)\in H^2_{0,\#}\left(\Omega\right)$. Then there exists a sufficiently large number λ_1, depending only on μ_1, μ_2, n, R, $\max_{ij}$, $\left\|a_{ij}\right\|_{C^1\left(\overline{\Omega}\right)}$, $\max_j\left\|b_j\right\|_{C\left(\overline{\Omega}\right)}$, $\left\|c\right\|_{C\left(\overline{\Omega}\right)}$, $\left\|\mathbf{n}\right\|_{C\left(\overline{\Omega}\right)}$ $\underline{k}$, $\overline{k}$, N such that the following Carleman estimate holds*

$$
\begin{aligned}
&\int_\Omega\left|L\left(W\left(\mathbf{x}\right)\right)+D_N^{-1}S_N\mathbf{n}^2(\mathbf{x})W(\mathbf{x})\right|^2\exp\left[2\lambda\left(z+3R\right)^{p_0}\right]d\mathbf{x}\\
&\geq C_3\lambda\int_\Omega\left(\left|\nabla W\right|^2+\lambda^2\left|W\right|^2\right)\exp\left[2\lambda\left(z+3R\right)^{p_0}\right]d\mathbf{x} \quad (2.2.36)
\end{aligned}
$$

for all $\lambda \geq \lambda_1$ *and* W *in* $H^2_{0,\#}(\Omega)$.

This Corollary follows immediately from Theorem 2.2.1 as well as from the well known fact (see, e.g. lemma 2.1 in [23]) that the Carleman estimate depends only on the principal part of a PDE operator while the lower order terms of this operator can be absorbed in this estimate.

2.2.2 A Carleman estimate on parabolic operators

Let the matrix A be as in (1.2.1). The main aim of this section is to prove a Carleman estimate in a general domain Ω. Similar versions of Carleman estimate can be found in [41, Theorem 3.1] and [46, Lemma 5] when Ω is an annulus and [40, Theorem 4.1] and when Ω is a cube. In this dissertation, we will use the following estimate to derive the convergence of the quasi-reversibility method. It can be deduced from [14, Lemma 3, Chapter 4, §1].

Without lost of generality, we can assume that

$$\Omega \subset \left\{ \mathbf{x} = (x_1, x_2, \ldots, x_d) : 0 < x_1 + X^{-2} \sum_{i=2}^{d} x_i^2 < 1 \right\} \tag{2.2.37}$$

for some $0 < X < 1$. Define the function

$$\psi(\mathbf{x}) = x_1 + \frac{1}{2X^2} \sum_{i=1}^{d} x_i^2 + \alpha, \quad 0 < \alpha < 1/2. \tag{2.2.38}$$

Using Lemma 3 in [30, Chapter 4, §1] for the function $u \in C^2(\overline{\Omega})$ that is independent of the time variable, we can find a constant σ_0 and a constant σ_1 (depending only on α and the entries a_{ij}, $1 \leq i, j \leq d$, of the matrix A) such that for all $\lambda \geq \sigma_0$ and $p > \sigma_1$

$$\begin{aligned} \frac{\lambda p}{X^2} e^{2\lambda\psi^{-p}(\mathbf{x})} |\nabla u|^2 + \lambda^3 p^4 \psi^{-2p-2} e^{2\lambda\psi^{-p}(\mathbf{x})} |u|^2 \leq -\frac{C\lambda p}{X^2} e^{2\lambda\psi^{-p}(\mathbf{x})} u \mathrm{Div}(A\nabla u) \\ + C\psi^{p+2} e^{2\lambda\psi^{-p}(\mathbf{x})} |\mathrm{Div}(A\nabla u)|^2 + \mathrm{Div} U \end{aligned} \tag{2.2.39}$$

for all $\mathbf{x} \in \Omega$ where the vector U satisfies

$$|U| \leq Ce^{2\lambda\psi^{-p}(\mathbf{x})} \left(\frac{\lambda p}{X} |\nabla u|^2 + \frac{\lambda^3 p^3}{X^3} \psi^{-2p-2} u^2 \right). \tag{2.2.40}$$

Applying (2.2.39) and (2.2.40), we have the lemma.

Lemma 2.2.1 (Carleman estimate)**.** *Let $u \in C^2(\overline{\Omega})$ satisfying*

$$u|_{\partial\Omega} = A\nabla u \cdot \nu = 0 \quad \text{on } \partial\Omega \tag{2.2.41}$$

where ν the outward unit normal vector of $\partial\Omega$. Then, there exist a positive number σ_0 and σ_1, depending only on α and A, such that

$$\begin{aligned} \frac{\lambda p}{X^2} \int_\Omega e^{2\lambda\psi^{-p}(\mathbf{x})} |\nabla u|^2 d\mathbf{x} + \lambda^3 p^4 \int_\Omega \psi^{-2p-2} e^{2\lambda\psi^{-p}(\mathbf{x})} |u|^2 d\mathbf{x} \\ \leq C \int_\Omega \psi^{p+2} e^{2\lambda\psi^{-p}(\mathbf{x})} |\mathrm{Div}(A\nabla u)|^2 d\mathbf{x} \end{aligned} \tag{2.2.42}$$

for $\lambda > \sigma_0$ and $p > \sigma_1$.

Proof. We claim that

$$\nabla u(\mathbf{x}) = 0 \quad \text{for all } \mathbf{x} \in \partial\Omega. \tag{2.2.43}$$

In fact, assume that $\nabla u(\mathbf{x}) \neq 0$ at some points $\mathbf{x} \in \partial\Omega$. Since $u(\mathbf{x}) = 0$ on $\partial\Omega$, see (2.2.41), $\nabla u(\mathbf{x}) \cdot \tau(\mathbf{x}) = 0$ where $\tau(\mathbf{x})$ is any tangent vector to $\partial\Omega$ at the point $\mathbf{x}$. Thus, $\nabla u(\mathbf{x})$ is perpendicular to $\partial\Omega$ at $\mathbf{x}$. In other words, $\nabla u(\mathbf{x}) = \theta\nu(\mathbf{x})$ for some nonzero scalar θ. We have $0 = A(\mathbf{x})\nabla u(\mathbf{x}) \cdot \nu(\mathbf{x}) = \theta A(\mathbf{x})\nu(\mathbf{x}) \cdot \nu(\mathbf{x})$, which is a contradiction to (1.2.2).

Integrating both sides of (2.2.39), we have

$$\frac{\lambda p}{X^2}\int_\Omega e^{2\lambda\psi^{-p}(\mathbf{x})}|\nabla u|^2 d\mathbf{x} + \lambda^3 p^4 \int_\Omega \psi^{-2p-2} e^{2\lambda\psi^{-p}(\mathbf{x})}|u|^2 d\mathbf{x}$$
$$\leq -\frac{C\lambda p}{X^2}\int_\Omega e^{2\lambda\psi^{-p}(\mathbf{x})} u\mathrm{Div}(A\nabla u) d\mathbf{x} + C\int_\Omega \psi^{p+2} e^{2\lambda\psi^{-p}(\mathbf{x})}|\mathrm{Div}(A\nabla u)|^2 d\mathbf{x}. \quad (2.2.44)$$

Here, the term $\int_\Omega \mathrm{Div}U d\mathbf{x}$ is dropped because it vanishes due the the divergence theorem, (2.2.41) and (2.2.43) Using the inequality $|ab| \leq \lambda p a^2 + \frac{1}{2\lambda p} b^2$

$$-\frac{C\lambda p}{X^2}\int_\Omega e^{2\lambda\psi^{-p}(\mathbf{x})} u\mathrm{Div}(A\nabla u) d\mathbf{x}$$
$$\leq \frac{C\lambda^2 p^2}{X^2}\int_\Omega e^{2\lambda\psi^{-p}(\mathbf{x})} u^2 d\mathbf{x} + \frac{C}{X^2}\int_\Omega e^{2\lambda\psi^{-p}(\mathbf{x})}|\mathrm{Div}(A\nabla u)|^2 d\mathbf{x}. \quad (2.2.45)$$

Combining (2.2.44) and (2.2.45), we obtain

$$\frac{\lambda p}{X^2}\int_\Omega e^{2\lambda\psi^{-p}(\mathbf{x})}|\nabla u|^2 d\mathbf{x} + \lambda^3 p^4 \int_\Omega \psi^{-2p-2} e^{2\lambda\psi^{-p}(\mathbf{x})}|u|^2 d\mathbf{x}$$
$$\leq C\int_\Omega \psi^{p+2} e^{2\lambda\psi^{-p}(\mathbf{x})}|\mathrm{Div}(A\nabla u)|^2 d\mathbf{x}.$$

The proof is complete. □

CHAPTER 3: THE INVERSE SOURCE PROBLEM FOR THE HELMHOLTZ EQUATION

3.1 The numerical method to solve Problems 1 and 2

Assume that in (1.1.8) $g(k) \neq 0, \forall k \in [\underline{k}, \overline{k}]$. Introduce the function $v(\mathbf{x}, k)$,

$$v(\mathbf{x}, k) = \frac{u(\mathbf{x}, k)}{g(k)}, \quad \mathbf{x} \in \Omega, k \in [\underline{k}, \overline{k}]. \tag{3.1.1}$$

Let L be the elliptic operator defined in (1.1.6). By (1.1.8)

$$L\left(v(\mathbf{x}, k)\right) + k^2 \mathbf{n}^2\left(\mathbf{x}\right) v(\mathbf{x}, k) = f(\mathbf{x}), \quad \mathbf{x} \in \Omega, k \in [\underline{k}, \overline{k}]. \tag{3.1.2}$$

To eliminate the unknown right hand side $f(\mathbf{x})$ from equation (3.1.2), we differentiate it with respect to k and obtain

$$L\left(\partial_k v(\mathbf{x}, k)\right) + k^2 \mathbf{n}^2(\mathbf{x}) \partial_k v(\mathbf{x}, k) + 2k \mathbf{n}^2(\mathbf{x}) v(\mathbf{x}, k) = 0, \quad \mathbf{x} \in \Omega, k \in [\underline{k}, \overline{k}]. \tag{3.1.3}$$

It follows from (1.1.11), (1.1.12) and (3.1.1) that in the case of Problem 1 the function v satisfies the following boundary conditions

$$v(\mathbf{x}, k) = \frac{F(\mathbf{x}, k)}{g(k)}, \quad \mathbf{x} \in \partial\Omega, k \in [\underline{k}, \overline{k}], \tag{3.1.4}$$

$$\partial_z v(\mathbf{x}, k) = \frac{G(\mathbf{x}, k)}{g(k)}, \quad \mathbf{x} \in \Gamma_+, k \in [\underline{k}, \overline{k}]. \tag{3.1.5}$$

In Problem 2 only condition (3.1.4) holds.

Fix an integer $N \geq 1$. Recalling the orthonormal basis $\{\Psi_r\}_{r=1}^{\infty}$ of $L^2(\underline{k}, \overline{k})$ in

Section 2.1, we approximate

$$v(\mathbf{x},k)=\sum_{m=1}^{N} v_m(\mathbf{x})\Psi_m(k) \quad \mathbf{x}\in\Omega, k\in[\underline{k},\overline{k}], \tag{3.1.6}$$

$$\partial_k v(\mathbf{x},k)=\sum_{m=1}^{N} v_m(\mathbf{x})\Psi'_m(k) \quad \mathbf{x}\in\Omega, k\in[\underline{k},\overline{k}], \tag{3.1.7}$$

where

$$v_m(\mathbf{x})=\int_{\underline{k}}^{\overline{k}} v(\mathbf{x},k)\Psi_m(k)dk \quad \mathbf{x}\in\Omega, m=1,2,\dots,N. \tag{3.1.8}$$

Remark 3.1.1. *Similarly with [16–18,24], we assume here that the truncated Fourier series* (3.1.6) *satisfies equation* (3.1.2) *and that truncated Fourier series* (3.1.6) *and* (3.1.7)*, taken together, satisfy equation* (3.1.3)*. This is our* ***approximate mathematical model****. Since we work with a numerical method, we accept this approximation scheme. Our main goal below is to find numerically Fourier coefficients* $v_m(\mathbf{x})$*,* $m=1,2,\dots,N$*, of* $v(\mathbf{x},k)$*, see* (3.1.8)*. If those Fourier coefficients are approximated, the target unknown function* $f(\mathbf{x})$ *can be approximated as the right hand side of* (3.1.2)*.*

Remark 3.1.2. *The number* N *is chosen numerically. Proving convergence of our method as* $N\to\infty$ *is very challenging and such proofs are very rare in the field of ill-posed problems. Indeed, the intrinsic reason of this is the ill-posedness of those problems. Therefore, we omit the proof of convergence of our method as* $N\to\infty$*. Nevertheless, a rich numerical experience of a number of previous publications, see, e.g. [16–18,24–28] indicates that this truncation technique still leads to good numerical results.*

We now compare numerically the true function $v(\mathbf{x},k)$ with its approximation (3.1.6). and observe that their difference is small, see Figure 3.1 for the illustration.

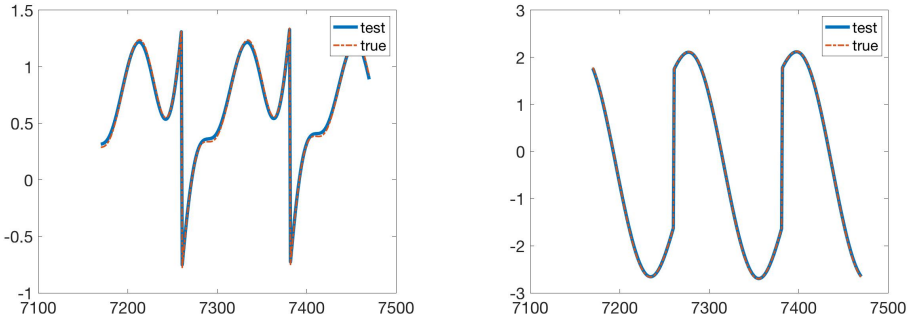

(a) The real parts of the true and test functions

(b) The imaginary parts of the true and test functions

Figure 3.1: The comparison of the true function $v(\cdot, k = 1.5) = \sum_{m=1}^{\infty} u_m(\mathbf{x})\Psi_m(k)$ and the test function $\sum_{m=1}^{10} v_m(\cdot)\Psi_n(k)$ in Test 5, see Section 2.2.1. In this test, we consider the case $n = 2$ and $\Omega = (-2, 2)^2$. On Ω, we arrange a uniform grid of 121×121 points in Ω. Those points are numbered from 1 to 121^2. In (a) and (b), we respectively show the real and imaginary parts of the two functions at 300 points numbered from 7170 to 7470. It is evident that reconstructing the first 10 terms of the Fourier coefficients of $v(\mathbf{x}, k)$ is sufficient to solve our inverse source problems.

Plugging (3.1.6) and (3.1.7) in equation (3.1.3), we obtain

$$\sum_{r=1}^{N} \left(Lv_r\left(\mathbf{x}\right)\right) \Psi_r'(k) + \sum_{r=1}^{N} \left(\mathbf{n}^2(\mathbf{x}) v_r\left(\mathbf{x}\right)\right) \left(k^2 \Psi_r'(k) + 2k\Psi_r(k)\right) = 0, \ \mathbf{x} \in \Omega. \quad (3.1.9)$$

For each $m = 1, ..., N$, we multiply both sides of (3.1.9) by the function $\Psi_m(k)$ and then integrate the resulting equation with respect to $k \in \left(\underline{k}, \overline{k}\right)$. We obtain

$$\sum_{r=1}^{N} \left(Lv_r\left(\mathbf{x}\right)\right) \int_{\underline{k}}^{\overline{k}} \Psi_r'(k)\Psi_m(k)dk + \sum_{r=1}^{N} \left(\mathbf{n}^2(\mathbf{x}) v_r\left(\mathbf{x}\right)\right) \int_{\underline{k}}^{\overline{k}} \left(k^2 \Psi_r'(k) + 2k\Psi_r(k)\right) \Psi_m(k)dk = 0 \quad (3.1.10)$$

for all $\mathbf{x} \in \Omega$, $m = 1, 2, \ldots, N$. Denote

$$V(\mathbf{x}) = (v_1(\mathbf{x}), v_2(\mathbf{x}), \cdots, v_N(\mathbf{x}))^T \quad \mathbf{x} \in \Omega, \quad (3.1.11)$$

$$S_N = (s_{mr})_{m,r=1}^N, \quad \text{with } s_{mr} = \int_{\underline{k}}^{\overline{k}} \left(k^2\Psi_r'(k) + 2k\Psi_r(k)\right)\Psi_m(k)dk. \tag{3.1.12}$$

Then, (2.1.4), (3.1.10)-(3.1.12) imply

$$D_N L\left(V\left(\mathbf{x}\right)\right) + S_N \mathbf{n}^2(\mathbf{x})V(\mathbf{x}) = 0, \quad \mathbf{x} \in \Omega, \tag{3.1.13}$$

Denote

$$\widetilde{F}(\mathbf{x}) = \left(\int_{\underline{k}}^{\overline{k}} \frac{F(\mathbf{x},k)}{g(k)}\Psi_1(k)dk, \ldots, \int_{\underline{k}}^{\overline{k}} \frac{F(\mathbf{x},k)}{g(k)}\Psi_N(k)dk\right)^T, \quad \mathbf{x} \in \partial\Omega, \tag{3.1.14}$$

$$\widetilde{G}(\mathbf{x}) = \left(\int_{\underline{k}}^{\overline{k}} \frac{G(\mathbf{x},k)}{g(k)}\Psi_1(k)dk, \ldots, \int_{\underline{k}}^{\overline{k}} \frac{G(\mathbf{x},k)}{g(k)}\Psi_N(k)dk\right)^T, \quad \mathbf{x} \in \Gamma_+. \tag{3.1.15}$$

It follows from (3.1.4) and (3.1.5) that in the case of 1 the vector function $V(\mathbf{x})$ satisfies the following two boundary conditions:

$$V\left(\mathbf{x}\right) = \widetilde{F}(\mathbf{x}), \ \mathbf{x} \in \partial\Omega, \tag{3.1.16}$$

and

$$\partial_\nu V\left(\mathbf{x}\right) = \widetilde{G}(\mathbf{x}), \ \mathbf{x} \in \Gamma_+. \tag{3.1.17}$$

And in the case of 2 only boundary condition (3.1.16) takes place.

These arguments lead to Algorithms 1 and 2 to solve Problems 1 and 2 respectively.

Algorithm 1 The procedure to solve Problem 1

1: Choose a number N. Construct the functions Ψ_m, $1 \leq m \leq N$, in Section 2.1 and compute the matrix D_N as in Proposition 2.1.1.
2: Calculate the boundary data $\widetilde{F}$ and $\widetilde{G}$ for the vector valued function V via (3.1.14) and (3.1.15) respectively.
3: Find an approximate solution of the system (3.1.13), (3.1.16) and (3.1.17) via the quasi-reversibility method.
4: Having $V = (v_1, v_2, \ldots, v_N)^T$ in hand, calculate $v_{\text{comp}}(\mathbf{x}, k)$ via (3.1.8).
5: Compute the reconstructed function f by (3.1.2).

Algorithm 2 The procedure to solve Problem 2

1: Choose a number N. Construct the functions Ψ_m, $1 \leq m \leq N$, in Section 2.1 and compute the matrix D_N as in Proposition 2.1.1.
2: Calculate the boundary data $\widetilde{F}$ for the vector valued function V via (3.1.14).
3: Solve the elliptic Dirichlet boundary value problem (3.1.13), (3.1.16).
4: Having $V = (v_1, v_2, \ldots, v_N)^T$ in hand, calculate $v_{\text{comp}}(\mathbf{x}, k)$ via (3.1.8).
5: Compute the reconstructed function f by (3.1.2).

In the next section, we briefly discuss the QRM used in Step 3 of Algorithm 1. We mention that the QRM is an efficient approach to solve partial differential equations with over-determined boundary data.

3.2 The quasi-reversibility method

In this section, we present the QRM for the numerical solution of Problem 1. By saying below that a vector valued function belongs to a Hilbert space, we mean that each of its components belongs to this space. The norm of this vector valued function in that Hilbert space is naturally defined as the square root of the sum of squares of norms of components. Recall that by Proposition 2.1.1 the matrix D_N is invertible. Therefore, by (3.1.13), (3.1.16) and (3.1.17) we need to find an approximate solution of the following over-determined boundary value problem with respect to the vector function $V(\mathbf{x})$

$$L\left(V\left(\mathbf{x}\right)\right) + D_N^{-1} S_N \mathbf{n}^2(\mathbf{x}) V(\mathbf{x}) = 0, \qquad \mathbf{x} \in \Omega, \tag{3.2.1}$$

$$V\left(\mathbf{x}\right) = \widetilde{F}(\mathbf{x}), \qquad \mathbf{x} \in \partial\Omega, \tag{3.2.2}$$

$$\partial_\nu V\left(\mathbf{x}\right) = \widetilde{G}(\mathbf{x}), \qquad \mathbf{x} \in \Gamma_+. \tag{3.2.3}$$

To do this, we consider the following minimization problem:

Problem 4 (Minimization Problem)**.** *Let* $\epsilon \in (0, 1)$

be the regularization parameter. Minimize the functional $J_\epsilon(V)$,

$$J_\epsilon(V) = \int_\Omega \left| L\left(V\left(\mathbf{x}\right)\right) + D_N^{-1} S_N \mathbf{n}^2(\mathbf{x}) V(\mathbf{x}) \right|^2 d\mathbf{x} + \epsilon \|V\|^2_{H^2(\Omega)}, \tag{3.2.4}$$

on the set of $N-D$ *vector valued functions* $V \in H^2\left(\Omega\right)$ *satisfying boundary conditions* (3.2.2) *and* (3.2.3).

We assume that the set of vector functions indicated in the formulation of this problem is non empty; i.e., we assume that there exists an $N-$D vector valued function Φ such that the set

$$\left\{ \Phi \in H^2\left(\Omega\right), \Phi \mid_{\partial\Omega} = \widetilde{F}(\mathbf{x}), \partial_\nu \Phi \mid_{\Gamma_+} = \widetilde{G}(\mathbf{x}) \right\}. \tag{3.2.5}$$

Theorem 3.2.1. *Assume that there exists an* $N-D$ *vector valued function* Φ *satisfying* (3.2.5). *Then for each* $\epsilon > 0$, *there exists a unique minimizer* $V_{\min,\epsilon} \in H^2(\Omega)$ *of the functional* J_ϵ *in* (3.2.4) *that satisfies boundary conditions* (3.2.2) *and* (3.2.3).

Proof. The proof of Theorem 3.2.1 is based on the variational principle and Riesz theorem. Let $(\cdot,\cdot)$ and $[\cdot,\cdot]$ denote scalar products in Hilbert spaces $L^2\left(\Omega\right)$ and $H^2\left(\Omega\right)$ respectively of $N-$D vector valued functions. For any vector valued function $V \in H^2\left(\Omega\right)$ satisfying boundary conditions (3.2.2) and (3.2.3), set

$$W(\mathbf{x}) = V(\mathbf{x}) - \Phi(\mathbf{x}), \quad \mathbf{x} \in \Omega. \tag{3.2.6}$$

By (3.2.5) $W \in H^2_{0,\#}\left(\Omega\right)$, where

$$H^2_{0,\#}\left(\Omega\right) = \left\{ w \in H^2\left(\Omega\right) : w \mid_{\partial\Omega} = 0, \partial_\nu w \mid_{\Gamma_+} = 0 \right\}. \tag{3.2.7}$$

Clearly $H^2_{0,\#}\left(\Omega\right)$ is a closed subspace of the space $H^2\left(\Omega\right)$. Let $V_{\min,\epsilon}$ be any minimizer

of the functional (3.2.4), if it exists. Denote

$$W_{\min,\epsilon} = V_{\min,\epsilon} - \Phi. \tag{3.2.8}$$

By the variational principle the following identity holds

$$\begin{aligned}\left(L\left(W_{\min,\epsilon}\left(\mathbf{x}\right)\right) + D_N^{-1}S_N\mathbf{n}^2(\mathbf{x})W_{\min,\epsilon}(\mathbf{x}), L\left(P\left(\mathbf{x}\right)\right) + D_N^{-1}S_N\mathbf{n}^2(\mathbf{x})P(\mathbf{x})\right)\\ + \epsilon\left[W_{\min,\epsilon}, P\right] = \left(L\left(\Phi\left(\mathbf{x}\right)\right) + D_N^{-1}S_N\mathbf{n}^2(\mathbf{x})\Phi(\mathbf{x}), L\left(P\left(\mathbf{x}\right)\right) + D_N^{-1}S_N\mathbf{n}^2(\mathbf{x})P(\mathbf{x})\right)\\ + \epsilon\left[\Phi, P\right], \end{aligned} \tag{3.2.9}$$

for all $P \in H^2_{0,\#}(\Omega)$. The left hand side of the identity (3.2.9) generates a new scalar product $\{\cdot,\cdot\}$ in the space $H^2_{0,\#}\left(\Omega\right)$. The corresponding norm $\{\cdot\}$ is equivalent to the standard norm $\|\cdot\|_{H^2(\Omega)}$. Hence, (3.2.9) is equivalent to

$$\begin{aligned}\left\{W_{\min,\epsilon}, P\right\} = \left(L\left(\Phi\left(\mathbf{x}\right)\right) + D_N^{-1}S_N\mathbf{n}^2(\mathbf{x})\Phi(\mathbf{x}), L\left(P\left(\mathbf{x}\right)\right) + D_N^{-1}S_N\mathbf{n}^2(\mathbf{x})P(\mathbf{x})\right)\\ + \epsilon\left[\Phi, P\right] \end{aligned} \tag{3.2.10}$$

for all $P \in H^2_{0,\#}\left(\Omega\right)$. On the other hand, the right hand side of (3.2.10) can be estimated as

$$\begin{aligned}\left|\left(L\left(\Phi\left(\mathbf{x}\right)\right) + D_N^{-1}S_N\mathbf{n}^2(\mathbf{x})\Phi(\mathbf{x}), L\left(P\left(\mathbf{x}\right)\right) + D_N^{-1}S_N\mathbf{n}^2(\mathbf{x})P(\mathbf{x})\right) + \epsilon\left[\Phi, P\right]\right|\\ \leq C_1\left\{\Phi\right\}\left\{P\right\}, \end{aligned}$$

where the number $C_1 = C_1\left(L, D_N^{-1}S_N, \mathbf{n}^2, \epsilon\right) > 0$ depends only on listed parameters. Hence, the right hand side of (3.2.10) can be considered as a bounded linear functional $l_\Phi\left(P\right) : H^2_0\left(\Omega\right) \to \mathbb{C}$. By Riesz theorem there exists unique vector function $Q \in$

$H^2_{0,\#}(\Omega)$ such that

$$\{W_{\min,\epsilon}, P\} = \{Q, P\}, \quad \text{for all } P \in H^2_{0,\#}(\Omega),$$

directly yielding the identity (3.2.10). As a consequence, $W_{\min,\epsilon}$ exists and; indeed, $W_{\min,\epsilon} = Q$. Finally, by (3.2.8) $V_{\min,\epsilon} = W_{\min,\epsilon} + \Phi$. □

The minimizer $V_{\min,\epsilon}$ of J_ϵ, subject to the constraints (3.2.2) and (3.2.3) is called the *regularized solution* of the problem (3.2.1), (3.2.2) and (3.2.3). In the theory of Ill-Posed Problems, it is important to prove convergence of regularized solutions to the true one as the noise in the data tends to zero [45]. In the next section, we establish a Carleman estimate for general elliptic operators. This estimate is essential for the proof of that convergence result in our problem, see Section 2.2.1.

3.3 Convergence Analysis

While Theorem 3.2.1 ensures the existence and uniqueness of the solution of the Minimization Problem (Problem 4), it does not claim convergence of minimizers, i.e. regularized solutions, to the exact solution as noise in the data tends to zero. At the same time such a convergence result is obviously important. However, this theorem is much harder to prove than Theorem 3.2.1. Indeed, while only the variational principle and Riesz theorem are used in the proof of Theorem 3.2.1, a different apparatus is required in the convergence analysis. This apparatus is based on the Carleman estimate of Theorem 2.2.1. Then we establish the convergence rate of minimizers.

Following one of the main principles of the regularization theory [45], we assume now that vector functions $\widetilde{F}(\mathbf{x})$ and $\widetilde{G}(\mathbf{x})$ in (3.2.2) and (3.2.3) are given with a noise. More precisely, let $\Phi(\mathbf{x}) \in H^2(\Omega)$ be the function defined in (3.2.5). We assume that this is given with a noise of the level $\delta \in (0,1)$, i.e.

$$\|\Phi^* - \Phi\|_{H^2(\Omega)} \leq \delta, \tag{3.3.1}$$

where the vector function $\Phi^* \in H^2(\Omega)$ corresponds to the noiseless data. In the case of noiseless data, we assume the existence of the solution $V^* \in H^2(\Omega)$ of the following analog of the problem (3.2.1)-(3.2.3):

$$L(V^*(\mathbf{x})) + D_N^{-1} S_N \mathbf{n}^2(\mathbf{x}) V^*(\mathbf{x}) = 0, \quad \mathbf{x} \in \Omega, \tag{3.3.2}$$

$$V^*(\mathbf{x}) = \widetilde{F}^*(\mathbf{x}), \ \mathbf{x} \in \partial\Omega, \tag{3.3.3}$$

$$\partial_\nu V^*(\mathbf{x}) = \widetilde{G}^*(\mathbf{x}), \ \mathbf{x} \in \Gamma_+. \tag{3.3.4}$$

Similarly to (3.2.5), we assume the existence of the vector valued function function Φ^* such that

$$\Phi^* \in H^2(\Omega), \Phi^*(\mathbf{x}) \mid_{\partial\Omega} = \widetilde{F}^*(\mathbf{x}), \ \partial_\nu \Phi^*(\mathbf{x}) \mid_{\Gamma_+} = \widetilde{G}^*(\mathbf{x}). \tag{3.3.5}$$

Similarly to (3.2.6), let

$$W^* = V^* - \Phi^*. \tag{3.3.6}$$

Then (3.2.7), (3.3.5) and (3.3.6) imply that $W^* \in H_0^2(\Omega)$. Also, using (3.3.2)-(3.3.5), we obtain

$$L(W^*(\mathbf{x})) + D_N^{-1} S_N \mathbf{n}^2(\mathbf{x}) (W^*(\mathbf{x})) = -L(\Phi^*(\mathbf{x})) - D_N^{-1} S_N \mathbf{n}^2(\mathbf{x}) (\Phi^*(\mathbf{x})), \quad \mathbf{x} \in \Omega. \tag{3.3.7}$$

Theorem 3.3.1 (The convergence rate)**.** *Assume that conditions of Theorem 3.2.1 as well as conditions (3.3.1)-(3.3.6) hold. Let λ_1 be the number of Corollary 2.2.1. Define the number η as*

$$\eta = 2(4R)^{p_0}. \tag{3.3.8}$$

Assume that the number $\delta_0 \in (0,1)$ *is so small that* $\ln \delta_0^{-1/\eta} > \lambda_1$. *Let* $\delta \in (0, \delta_0)$. *Set* $\epsilon = \epsilon(\delta) = \delta^2$. *Let* $V_{\min,\epsilon(\delta)} \in H^2(\Omega)$ *be the unique minimizer of the functional (3.2.4) which is found in Theorem 3.2.1. Then the following convergence rate of regularized solutions holds*

$$\left\| V_{\min,\epsilon(\delta)} - V^* \right\|_{H^1(\Omega)} \leq C_4 \left(1 + \|W^*\|_{H^2(\Omega)} \right) \sqrt{\delta}, \tag{3.3.9}$$

where the $C_4 > 0$ *depends on* μ_1, μ_2, n, R, $\max_{ij}$, $\|a_{ij}\|_{C^1(\overline{\Omega})}$, $\max_j \|b_j\|_{C(\overline{\Omega})}$, $\|c\|_{C(\overline{\Omega})}$, $\|\mathbf{n}\|_{C(\overline{\Omega})}$ $\underline{k}$, $\overline{k}$, N.

Proof. We use in this proof the Carleman estimate of Corollary 2.2.1. Similarly with (3.2.8) let $V_{\min,\epsilon(\delta)} - \Phi = W_{\min,\epsilon(\delta)} \in H^2_{0,\#}(\Omega)$. We now rewrite (3.2.9) as

$$\begin{aligned} &\left(L\left(W_{\min,\epsilon(\delta)}(\mathbf{x}) \right) + D_N^{-1} S_N \mathbf{n}^2(\mathbf{x}) W_{\min,\epsilon(\delta)}(\mathbf{x}), L(P(\mathbf{x})) + D_N^{-1} S_N \mathbf{n}^2(\mathbf{x}) P(\mathbf{x}) \right) \\ &+\epsilon(\delta) \left[W_{\min,\epsilon(\delta)}, P \right] = \left(L(\Phi(\mathbf{x})) + D_N^{-1} S_N \mathbf{n}^2(\mathbf{x}) \Phi(\mathbf{x}), L(P(\mathbf{x})) + D_N^{-1} S_N \mathbf{n}^2(\mathbf{x}) P(\mathbf{x}) \right) \\ &+ \epsilon(\delta) [\Phi, P], \end{aligned} \tag{3.3.10}$$

for all $P \in H^2_{0,\#}(\Omega)$. Also, we rewrite (3.3.7) in an equivalent form,

$$\begin{aligned} &\left(L(W^*(\mathbf{x})) + D_N^{-1} S_N \mathbf{n}^2(\mathbf{x}) W^*(\mathbf{x}), L(P(\mathbf{x})) + D_N^{-1} S_N \mathbf{n}^2(\mathbf{x}) P(\mathbf{x}) \right) + \epsilon(\delta) [W^*, P] \\ &= \left(L(\Phi^*(\mathbf{x})) + D_N^{-1} S_N \mathbf{n}^2(\mathbf{x}) \Phi^*(\mathbf{x}), L(P(\mathbf{x})) + D_N^{-1} S_N \mathbf{n}^2(\mathbf{x}) P(\mathbf{x}) \right) \\ &+ \epsilon(\delta) [W^*, P], \end{aligned} \tag{3.3.11}$$

for all $P \in H^2_{0,\#}(\Omega)$. Denote

$$\widetilde{W} = W_{\min,\epsilon(\delta)} - W^* \in H^2_{0,\#}(\Omega), \ \widetilde{\Phi} = \Phi - \Phi^*.$$

Subtracting (3.3.11) from (3.3.10), we obtain

$$\begin{aligned}&\left(\left(L\left(\widetilde{W}\left(\mathbf{x}\right)\right)+D_N^{-1}S_N\mathbf{n}^2(\mathbf{x})\widetilde{W}(\mathbf{x}),L\left(P\left(\mathbf{x}\right)\right)+D_N^{-1}S_N\mathbf{n}^2(\mathbf{x})P(\mathbf{x})\right)+\epsilon\left(\delta\right)\left[\widetilde{W},P\right]\right)\\&=\left(L\left(\widetilde{\Phi}\left(\mathbf{x}\right)\right)+D_N^{-1}S_N\mathbf{n}^2(\mathbf{x})\widetilde{\Phi}(\mathbf{x}),L\left(P\left(\mathbf{x}\right)\right)+D_N^{-1}S_N\mathbf{n}^2(\mathbf{x})P(\mathbf{x})\right)+\epsilon\left(\delta\right)\left[W^*,P\right],\end{aligned}$$

for all $P\in H^2_{0,\#}(\Omega)$. Setting here $P=\widetilde{W}$ and using Cauchy-Schwarz inequality and (3.3.1), we obtain

$$\int_\Omega\left|L\left(\widetilde{W}\left(\mathbf{x}\right)\right)+D_N^{-1}S_N\mathbf{n}^2(\mathbf{x})\widetilde{W}(\mathbf{x})\right|^2d\mathbf{x}\leq C_4\delta^2\left(1+\|W^*\|^2_{H^2(\Omega)}\right).\tag{3.3.12}$$

We now want to apply Corollary 2.2.1. We have

$$\begin{aligned}&\int_\Omega\left|L\left(\widetilde{W}\left(\mathbf{x}\right)\right)+D_N^{-1}S_N\mathbf{n}^2(\mathbf{x})\widetilde{W}(\mathbf{x})\right|^2d\mathbf{x}\\&=\int_\Omega\left|L\left(\widetilde{W}\left(\mathbf{x}\right)\right)+D_N^{-1}S_N\mathbf{n}^2(\mathbf{x})\widetilde{W}(\mathbf{x})\right|^2\exp\left(2\lambda\left(z+3R\right)^{p_0}\right)\exp\left(-2\lambda\left(z+3R\right)^{p_0}\right)d\mathbf{x}\\&\geq\exp\left(-2\lambda\left(4R\right)^{p_0}\right)\int_\Omega\left|L\left(\widetilde{W}\left(\mathbf{x}\right)\right)+D_N^{-1}S_N\mathbf{n}^2(\mathbf{x})\widetilde{W}(\mathbf{x})\right|^2\exp\left(2\lambda\left(z+3R\right)^{p_0}\right)d\mathbf{x}.\end{aligned}$$

Substituting this into (3.3.12), we obtain

$$\begin{aligned}&\int_\Omega\left|L\left(\widetilde{W}\left(\mathbf{x}\right)\right)+D_N^{-1}S_N\mathbf{n}^2(\mathbf{x})\widetilde{W}(\mathbf{x})\right|^2\exp\left(2\lambda\left(z+3R\right)^{p_0}\right)d\mathbf{x}\\&\qquad\leq C_4\delta^2\left(1+\|W^*\|^2_{H^2(\Omega)}\right)\exp\left(2\lambda\left(4R\right)^{p_0}\right).\end{aligned}\tag{3.3.13}$$

By Corollary 2.2.1 the left hand side of inequality (3.3.13) can be estimated for any

$\lambda \geq \lambda_1$ as

$$\begin{aligned}\int_\Omega \left|L\left(\widetilde{W}\left(\mathbf{x}\right)\right) + D_N^{-1} S_N \mathbf{n}^2(\mathbf{x}) \widetilde{W}(\mathbf{x})\right|^2 \exp\left(2\lambda\left(z+3R\right)^{p_0}\right) d\mathbf{x} \\ \geq & C_3\lambda \int_\Omega \left(\left|\nabla \widetilde{W}\right|^2 + \lambda^2 \left|\widetilde{W}\right|^2\right) \exp\left[2\lambda\left(z+3R\right)^{p_0}\right] d\mathbf{x} \\ \geq & \, C_4 \exp\left[2\lambda\left(2R\right)^{p_0}\right] \|W\|^2_{H^1(\Omega)}.\end{aligned}$$

Comparing this with (3.3.13), we obtain

$$\|\widetilde{W}\|^2_{H^1(\Omega)} \leq C_4 \delta^2 \left(1 + \|W^*\|^2_{H^2(\Omega)}\right) \exp\left(2\lambda\left(4R\right)^{p_0}\right). \tag{3.3.14}$$

Set $\epsilon = \delta^2$. Next, choose $\lambda = \lambda(\delta)$ such that $\exp\left(2\lambda\left(4R\right)^{p_0}\right) = 1/\delta$. Hence,

$$\lambda = \lambda(\delta) = \ln \delta^{-1/\eta}, \tag{3.3.15}$$

where the number η is defined in (3.3.8). This choice is possible since $\delta \in (0, \delta_0)$ and $\ln \delta_0^{-1/\eta} > \lambda_1$, implying that $\lambda(\delta) > \lambda_1$. Thus, (3.3.14) and (3.3.15) imply that

$$\|\widetilde{W}\|_{H^1(\Omega)} \leq C_4 \left(1 + \|W^*\|_{H^2(\Omega)}\right) \sqrt{\delta}. \tag{3.3.16}$$

Next, using triangle inequality, (3.3.16) and (3.3.1), we obtain

$$C_4 \left(1 + \|W^*\|_{H^2(\Omega)}\right) \sqrt{\delta} \geq \|\widetilde{W}\|_{H^1(\Omega)} = \left\|\left(V_{\min,\epsilon(\delta)} - V^*\right) - \left(\Phi - \Phi^*\right)\right\|_{H^1(\Omega)}$$

$$\geq \left\|V_{\min,\epsilon(\delta)} - V^*\right\|_{H^1(\Omega)} - \|\Phi - \Phi^*\|_{H^1(\Omega)} \geq \left\|V_{\min,\epsilon(\delta)} - V^*\right\|_{H^1(\Omega)} - \delta.$$

Hence,

$$\left\|V_{\min,\epsilon(\delta)} - V^*\right\|_{H^1(\Omega)} \leq \delta + C_4 \left(1 + \|W^*\|_{H^2(\Omega)}\right) \sqrt{\delta} \leq C_4 \left(1 + \|W^*\|_{H^2(\Omega)}\right) \sqrt{\delta}. \tag{3.3.17}$$

Numbers C_4 in middle and right inequalities (3.3.17) are different and depend only on μ_1, μ_2, n, R, $\max_{ij}$, $\|a_{ij}\|_{C^1(\overline{\Omega})}$, $\max_j \|b_j\|_{C(\overline{\Omega})}$, $\|c\|_{C(\overline{\Omega})}$, $\|\mathbf{n}\|_{C(\overline{\Omega})}$ $\underline{k}$, $\overline{k}$, N. The target estimate (3.3.9) of this theorem follows from (3.3.17) immediately. $\square$

3.4 Numerical illustrations

In this section, we test our method in the 2-D case. The domain Ω is set to be the square

$$\Omega = (-R, R)^2$$

where $R = 2$. Let $M_{\mathbf{x}} = 120$ and $h_{\mathbf{x}} = 2R/M_{\mathbf{x}}$. We arrange a uniform grid of $(M_{\mathbf{x}} + 1) \times (M_{\mathbf{x}} + 1)$ points $\{\mathbf{x}_{ij}\}_{i,j=1}^{M_{\mathbf{x}}+1} \subset \overline{\Omega}$ where

$$\mathbf{x}_{ij} = (-R + (i-1)h_{\mathbf{x}}, -R + (j-1)h_{\mathbf{x}}). \tag{3.4.1}$$

In this section, we set $\underline{k} = 1.5$ and $\overline{k} = 4.5$. The interval $[\underline{k}, \overline{k}]$ is uniformly divided into $M_k = 150$ sub-intervals whose end points are given by

$$k_1 = \underline{k} < k_2 < k_3 < \cdots < k_{M_k+1} = \overline{k} \tag{3.4.2}$$

where $k_i = k_1 + (i-1)h_k$ and $h_k = (\overline{k} - \underline{k})/M_k$.

In all numerical tests of this section we computationally simulate the data for the inverse problem via solving equation (1.1.8) in the square Ω and with the boundary condition at $\partial\Omega$ generated by (1.1.9), i.e.

$$\partial_\nu u(\mathbf{x}, k) - iku(\mathbf{x}, k) = 0 \text{ for } \mathbf{x} \in \partial\Omega.$$

Hence, we do not specify in this section the operator L and the function $\mathbf{n}^2(\mathbf{x})$ outside of Ω. For brevity, we consider only the isotropic case, i.e. $L = \Delta$ for $\mathbf{x} \in \Omega$. To show that our method is applicable for the case of non homogeneous media, we choose the

function $\mathbf{n}^2(\mathbf{x})$ in all numerical tests below as:

$$\mathbf{n}^2(\mathbf{x}) = 1 + \frac{0.1\sin(3|\mathbf{x}|^2)}{3|\mathbf{x}|^2+1} \quad \text{for all } \mathbf{x} \in \Omega.$$

We choose $N = 10$ in (3.1.8) by a trial and error procedure. If, for example $N = 5$, then our reconstructed functions $f(\mathbf{x})$ are not satisfactory. Choosing $N > 10$ does not help us to enhance the accuracy of computed functions. We also refer here to Figure 3.1.

Remark 3.4.1 (The choice for the interval of wave numbers)**.** *The length of each side of the square* Ω *is* $2R = 4$ *units. We choose the longest wavelength* $\widetilde{\lambda}_{long} = 2\pi/\underline{k} = 2\pi/1.5 = 4.19$ *which is about* 4 *units. The upper bound of the wave number* $\overline{k} = 4.5$ *is set so that the shortest wavelength* $\widetilde{\lambda}_{short} = 1.39$ *is in the range that is compatible to the maximal* $l_{\max}$ *and minimal* $l_{\min}$ *sizes of the tested inclusions. More precisely, we choose* $\widetilde{\lambda}_{short} \in (0.7l_{\max}, 1.45l_{\min})$ *and* $\widetilde{\lambda}_{long}/\widetilde{\lambda}_{short} \approx 3$.

3.4.1 The forward problem

To generate the computationally simulated data (1.1.11), (1.1.12), we need to solve numerically the forward problem (1.1.8), (1.1.9). To avoid solving this problem in the entire space $\mathbb{R}^2$, we solve the following boundary value problem:

$$\begin{cases} \Delta u(\mathbf{x},k) + k^2\mathbf{n}^2(\mathbf{x})u(\mathbf{x},k) &= g(k)f(\mathbf{x}) \quad \mathbf{x} \in \Omega, \\ \partial_n u(\mathbf{x},k) - \mathrm{i}ku(\mathbf{x},k) &= 0 \qquad\quad \mathbf{x} \in \partial\Omega, \end{cases} \tag{3.4.3}$$

assuming that it has unique solution $u(\mathbf{x},k) \in C^2\left(\overline{\Omega}\right)$ for all $k \in [\underline{k},\overline{k}]$. We solve problem (3.4.3) by the finite difference method. Having computed the function $u(\mathbf{x},k)$, we extract the noisy data,

$$F(\mathbf{x},k) = u(\mathbf{x},k)(1 + \delta(-1+2\mathrm{rand}) + \mathrm{i}\delta(-1+2\mathrm{rand})),\ \mathbf{x} \in \partial\Omega, \tag{3.4.4}$$

$$G(\mathbf{x},k)=\partial_z u(\mathbf{x},k)(1+\delta(-1+2\text{rand})+\mathrm{i}\delta(-1+2\text{rand})),\ \mathbf{x}\in\Gamma_+, \tag{3.4.5}$$

see (1.1.11), (1.1.12). Here $\delta\in(0,1)$ is the noise level and "rand" is the function taking uniformly distributed random numbers in $[0,1]$. In this dissertation, we test our method with the noise level $\delta=0.05$, which means 5% noise.

Remark 3.4.2. *Recall that while in Problem 1 we use both functions $F(\mathbf{x},k)$ and $G(\mathbf{x},k)$ in (3.4.4), (3.4.5), in Problem 2 we use only the Dirichlet boundary condition $F(\mathbf{x},k)$, see (1.1.11)-(1.1.13). However, it follows from boundary condition (3.4.3) that the Neumann boundary condition is $\partial_\nu u(\mathbf{x},k)\mid_{\partial\Omega}=ikF(\mathbf{x},k)$. This explains why we computationally observe the uniqueness of our numerical solution of Problem 2.*

3.4.2 The inverse problem

In this section we describe the numerical implementation of the minimization procedure for the functional J_ϵ. We use the following form of the functionals J_ϵ:

$$J_\epsilon(V)=\int_\Omega |D_N\Delta V+S_N\mathbf{n}^2(\mathbf{x})V|^2d\mathbf{x}+\epsilon\|V\|^2_{L^2(\Omega)}. \tag{3.4.6}$$

This functional J_ϵ in (3.4.6) is slightly different from the one in (3.2.4). First, we do not use here the matrix D_N^{-1}. Indeed, this matrix is convenient to use for the above theoretical results. However, it is inconvenient to use in computations since it contains large numbers at $N=10$. Second, we replace the term $\|V\|^2_{H^2(\Omega)}$ in (3.2.4) by the term $\|V\|^2_{L^2(\Omega)}$. This is because the $L^2(\Omega)-$norm is easier to work with computationally than the $H^2(\Omega)-$norm. On the other hand, we have not observed any instabilities probably because the number 121×121 of grid points we use is not too large and all norms in finite dimensional spaces are equivalent. The regularization parameter ϵ in our computations was found by a trial and error procedure, $\epsilon=10^{-5}$.

We write derivatives involved in (3.4.6) via finite differences. Next, we minimize

the resulting functional with respect to values of the vector valued function

$$V(\mathbf{x}) = (v_1(\mathbf{x}), v_2(\mathbf{x}), \ldots, v_N(\mathbf{x}))^T$$

at grid points. The finite difference approximation of the functional $J_\epsilon(V)$ is

$$\begin{aligned} J_\epsilon(V) \quad &= h_{\mathbf{x}}^2 \sum_{i,j=2}^{M_{\mathbf{x}}} \sum_{m=1}^{N} \Big| \sum_{r=1}^{N} \Big\{ \frac{d_{mr}}{h_{\mathbf{x}}^2} \big[v_r(x_{i-1}, y_j) + v_r(x_{i+1}, y_j) \\ &\quad + v_r(x_i, y_{j-1}) + v_r(x_i, y_{j+1}) - 4v_r(x_i, y_j) \big] \\ &\quad + \mathbf{n}^2(x_i, y_j) s_{mr} v_r(x_i, y_j) \Big\} \Big|^2 + \epsilon h_{\mathbf{x}}^2 \sum_{i,j=1}^{M_{\mathbf{x}}+1} \sum_{m=1}^{N} |v_m(x_i, y_j)|^2, \end{aligned}$$

where d_{mn} and s_{mn} are elements of matrices D_N and S_N in (2.1.3) and (3.1.12) respectively. Introduce the "line up" version of the set $\{v_n(x_i, y_j) : 1 \le i, j \le M_{\mathbf{x}} + 1, 1 \le n \le N\}$ as the $(M_{\mathbf{x}} + 1)^2 N$ dimensional vector $\mathcal{V}$ with

$$\mathcal{V}_{\mathfrak{m}} = v_m(x_i, y_j) \quad 1 \le i, j \le M_{\mathbf{x}} + 1, 1 \le m \le N, \tag{3.4.7}$$

where

$$\mathfrak{m} = (i-1)(M_{\mathbf{x}} + 1)N + (j-1)N + m. \tag{3.4.8}$$

It is not hard to check that the map

$$\{1, \ldots, M_{\mathbf{x}} + 1\} \times \{1, \ldots, M_{\mathbf{x}} + 1\} \times \{1, \ldots, N\} \to \{1, \ldots, (M_{\mathbf{x}} + 1)^2 N\}$$

that sends (i, j, m) to $\mathfrak{m}$ as in (3.4.8) is onto and one-to-one. The functional $J_\epsilon(V)$ is rewritten in terms of the line up vector $\mathcal{V}$ as

$$\mathcal{J}_\epsilon(\mathcal{V}) = h_{\mathbf{x}}^2 |\mathcal{L}\mathcal{V}|^2 + \epsilon h_{\mathbf{x}}^2 |\mathcal{V}|^2$$

where $\mathcal{L}$ is the $(M_{\mathbf{x}} + 1)^2 N \times (M_{\mathbf{x}} + 1)^2 N$ matrix defined as follows. For each $\mathfrak{m} =$

$(i-1)(M_{\mathbf{x}}+1)N+(j-1)N+m$, $2 \le i,j \le M_{\mathbf{x}}$, $1 \le m \le N$,

1. set $\mathcal{L}_{\mathfrak{mn}} = -\frac{4d_{mn}}{h_{\mathbf{x}}^2} + \mathbf{n}^2(x_i,y_j)b_{mn}$, if $\mathfrak{n} = (i-1)(M_{\mathbf{x}}+1)N+(j-1)N+n, 1 \le n \le N$;

2. set $\mathcal{L}_{\mathfrak{mn}} = \frac{1}{h_{\mathbf{x}}^2}$ if $\mathfrak{n} = (i \pm 1 - 1)(M_{\mathbf{x}}+1)N+(j-1)N+n$ or $\mathfrak{n} = (i-1)(M_{\mathbf{x}}+1)N+(j \pm 1 - 1)N+n$, $1 \le n \le N$.

It is obvious that the minimizer of $\mathcal{J}_\epsilon$ satisfies the equation

$$(\mathcal{L}^*\mathcal{L} + \epsilon \mathrm{Id})\mathcal{V} = \vec{0}. \tag{3.4.9}$$

Here, $\vec{0}$ is the $(M_{\mathbf{x}}+1)^2N$ dimensional zero vector.

Next, we consider the "line up" version of the first condition in (3.1.16). The following information is available

$$\mathcal{V}_{\mathfrak{m}} = \tilde{F}_N(x_i,y_j,m),$$

where $\mathfrak{m}$ is as in (3.4.8). Hence, let $\mathcal{D}$ be the $(M_{\mathbf{x}}+1)^2N \times (M_{\mathbf{x}}+1)^2N$ diagonal matrix with such $\mathfrak{m}^{\text{th}}$ diagonal entries taking value 1 while the others are 0. This Dirichlet boundary constraint of the vector $\mathcal{V}$ become

$$\mathcal{D}\mathcal{V} = \tilde{\mathcal{F}}. \tag{3.4.10}$$

Here, the vector $\tilde{\mathcal{F}}$ is the "line up" vector of the data F_N in the same manner when we defined $\mathcal{V}$, see (3.4.8).

We implement the constraint of V in (3.1.17). This constraint allows us to collect the following information

$$\frac{\mathcal{V}_{\mathfrak{m}} - \mathcal{V}_{\mathfrak{m}'}}{h_{\mathbf{x}}} = \tilde{G}_N(x_i,y_j,m) \tag{3.4.11}$$

where $\mathfrak{m}$ is as in (3.4.8) and

$$\mathfrak{m}' = (i-1)(M_{\mathbf{x}}+1)N + (j-2)N + m \tag{3.4.12}$$

for $1 \leq i \leq M_{\mathbf{x}}+1$ and $j = M_{\mathbf{x}}+1$. We rewrite (3.4.11) as

$$\mathcal{N}\mathcal{V} = \tilde{\mathcal{G}} \tag{3.4.13}$$

where $\tilde{\mathcal{G}}$ is the "line up" version of $\tilde{G}_N$ and the matrix $\mathcal{N}$ is defined as

1. $\mathcal{N}_{\mathfrak{m}\mathfrak{m}} = 1/h_{\mathbf{x}}$ and $\mathcal{N}_{\mathfrak{m}\mathfrak{m}'} = -1/h_{\mathbf{x}}$ for $\mathfrak{m}$ and $\mathfrak{m}'$ given by (3.4.8) and (3.4.12) respectively, $1 \leq i \leq M_{\mathbf{x}}+1, j = M_{\mathbf{x}}+1$.

2. Other entries of $\mathcal{N}$ are 0.

In practice, we compute $\mathcal{V}$ by solving

$$\left(\begin{bmatrix} \mathcal{L} \\ \mathcal{D} \\ \mathcal{N} \end{bmatrix}^T \begin{bmatrix} \mathcal{L} \\ \mathcal{D} \\ \mathcal{N} \end{bmatrix} + \epsilon \mathrm{Id} \right) \mathcal{V} = \begin{bmatrix} \mathcal{L} \\ \mathcal{D} \\ \mathcal{N} \end{bmatrix}^T \begin{bmatrix} \vec{0} \\ \tilde{\mathcal{F}} \\ \tilde{\mathcal{G}} \end{bmatrix} \tag{3.4.14}$$

in the case of Problem 1 and we solve

$$\left(\begin{bmatrix} \mathcal{L} \\ \mathcal{D} \end{bmatrix}^T \begin{bmatrix} \mathcal{L} \\ \mathcal{D} \end{bmatrix} + \epsilon \mathrm{Id} \right) \mathcal{V} = \begin{bmatrix} \mathcal{L} \\ \mathcal{D} \end{bmatrix}^T \begin{bmatrix} \vec{0} \\ \tilde{\mathcal{F}} \end{bmatrix} \tag{3.4.15}$$

for Problem 2. Having the vector $\mathcal{V}$, we can compute the vector V_N via (3.4.7). Then, we follow Steps 4 and 5 of Algorithms 1 and Algorithms 2 to compute the functions v_{comp} via (3.1.6) and then f^{comp} by taking the real part of (3.1.2) when $k = 1.5$.

Remark 3.4.3 (Remark on Problem 2)**.** *We use* (3.4.15) *only for the convenience, since we do not want to have a significant extra programming effort, given that we*

have the computer code for solving (3.4.14).

3.4.3 Tests

In the cases of Test 1 and Test 2, we apply below our method for Problem 1. And in the cases of Tests 3-5 we apply our method for Problem 2. Whenever we say below about the accuracy of values of positive and negative parts of inclusions, we compare maximal positive values and minimal negative values of computed ones with true ones. Postprocessing was not applied in all tests presented below.

1. *Test 1. Problem 1. Two inclusions with different shapes.* The function f_{true} is given by

$$f_{\text{true}} = \begin{cases} 2.5 & \text{if } \max\{0.6|x-0.75|, |y|\} < 1.1, \\ -2 & \text{if } (x+0.75)^2 + y^2 < 0.55^2, \\ 0 & \text{otherwise,} \end{cases}$$

   and $g_{\text{true}}(k) = \mathrm{i}k$ for $k \in [\underline{k}, \overline{k}]$. We test the reconstructions of the locations, shapes and positive/negative values of the function f for two different inclusions. One of them is a rectangle and the other one is a disk. In this case, the function f_{true} attains both positive and negative values. The numerical solution for this case is displayed on Figure 3.2.

   It is evident that, for this test, our method for 1 provides good numerical results. The reconstructed locations, shapes as well as the positive/negative values of the function f^{comp} are of a good quality.

2. *Test 2.Problem 1. Four circular inclusions.* We consider the case when the

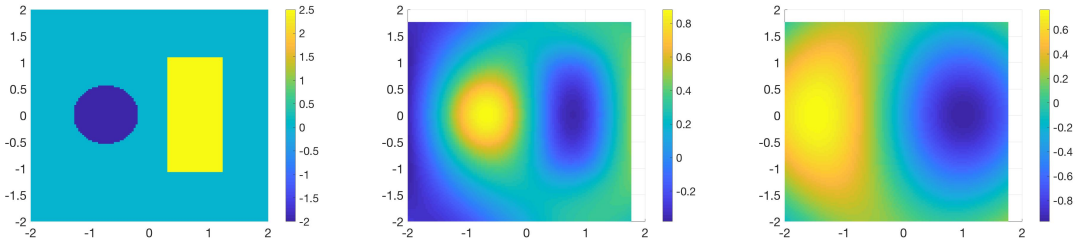

(a) The function f_{true}

(b) The real part of the function $v_{\text{true}}(\cdot, k = 1.5)$

(c) The imaginary part of the function $v_{\text{true}}(\cdot, k = 1.5)$

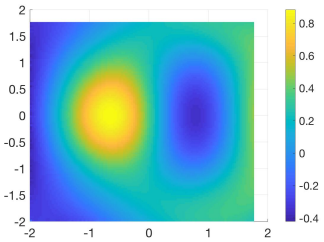

(d) The real part of the function $v_{\text{comp}}(\cdot, k = 1.5)$

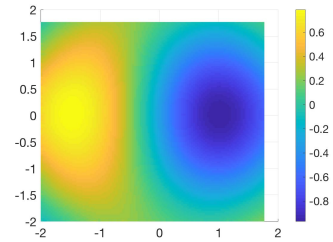

(e) The imaginary part of the function $v_{\text{comp}}(\cdot, k = 1.5)$

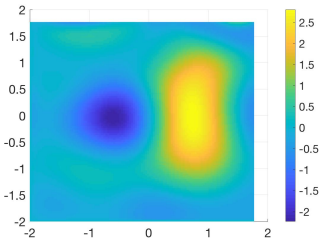

(f) The function f_{comp}

Figure 3.2: Test 1. The true and reconstructed source functions and the true and reconstructed functions $v(\mathbf{x}, k) = u(\mathbf{x}, k)/g(k)$ when $k = 1.5$. The reconstructed positive value of the source function is 2.76 (relative error 10.5%). The reconstructed negative value of the source function is -2.17 (relative error 8.5%).

function f_{true} is given by

$$f_{\text{true}} = \begin{cases} 1, & \text{if } (x-0.8)^2 + (y-0.8)^2 < 0.55^2 \\ & \text{or } (x+0.8)^2 + (y-0.8)^2 < 0.55^2, \\ -1, & \text{if } (x-0.8)^2 + (y+0.8)^2 < 0.55^2 \\ & \text{or } (x+0.8)^2 + (y+0.8)^2 < 0.55^2, \\ 0, & \text{otherwise,} \end{cases}$$

and $g_{\text{true}}(k) = 1$ for all $k \in [\underline{k}, \overline{k}]$. We test the model with four circular inclusions. The source function $f = 1$ in the two "upper" inclusion and $f = -1$ in the two "lower" inclusions.

The reconstruction is displayed in Figure 3.3. The source function is recon-

structed well in the sense of locations, shapes and values.

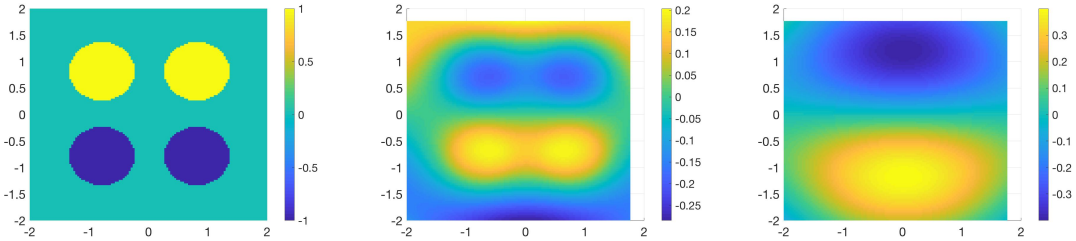

(a) The function f_{true}

(b) The real part of the function $v_{\text{true}}(\cdot, k = 1.5)$

(c) The imaginary part of the function $v_{\text{true}}(\cdot, k = 1.5)$

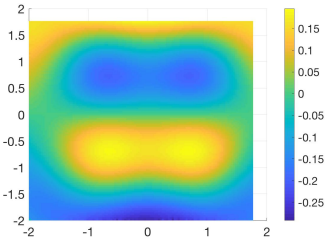

(d) The real part of the function $v_{\text{comp}}(\cdot, k = 1.5)$

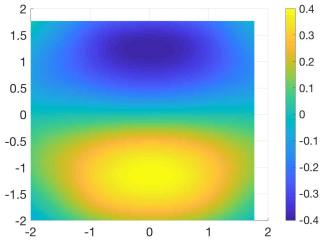

(e) The imaginary part of the function $v_{\text{comp}}(\cdot, k = 1.5)$

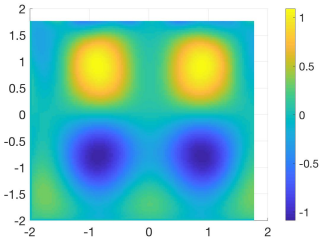

(f) The function f_{comp}

Figure 3.3: Test 2. The true and reconstructed source functions and the true and reconstructed functions $v(\mathbf{x}, k) = u(\mathbf{x}, k)/g(k)$ when $k = 1.5$. The reconstructed positive value of the source function is 1.11 (relative error 11.1%). The reconstructed negative value of the source function is -1.11 (relative error 11.1%).

3. *Test 3. Problem 2. A void in the square.* We consider the case when the negative part of the true source function f is surrounded by a square and f is positive in this square. More precisely,

$$f_{\text{true}} = \begin{cases} 1 & \text{if } \max\{|x|, |y|\} < 1.2 \text{ and } x^2 + y^2 \geq 0.48^2, \\ -1 & \text{if } x^2 + y^2 < 0.48^2, \\ 0 & \text{otherwise,} \end{cases}$$

and $g_{\text{true}}(k) = k$ for all $k \in [\underline{k}, \overline{k}]$.

The true f_{true} and computed f^{comp} source functions are displayed in Figure 3.4. We can see computed shapes of the “positive" square and the “negative" disk

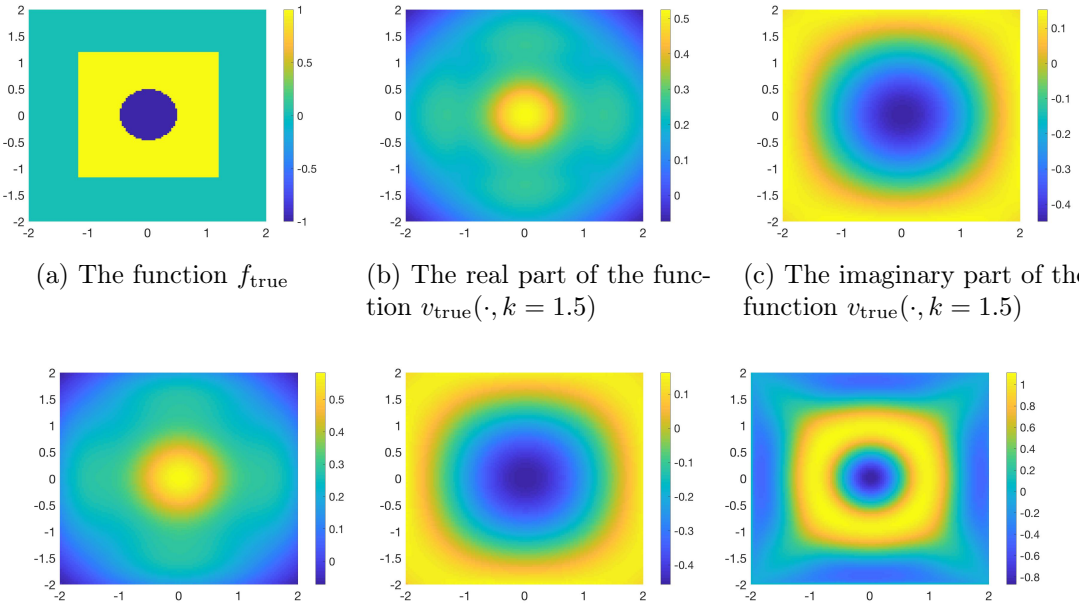

(a) The function f_{true}

(b) The real part of the function $v_{\text{true}}(\cdot, k = 1.5)$

(c) The imaginary part of the function $v_{\text{true}}(\cdot, k = 1.5)$

(d) The real part of the function $v_{\text{comp}}(\cdot, k = 1.5)$

(e) The imaginary part of the function $v_{\text{comp}}(\cdot, k = 1.5)$

(f) The function f_{comp}

Figure 3.4: Test 3. The true and reconstructed source functions and the true and reconstructed functions $v(\mathbf{x}, k) = u(\mathbf{x}, k)/g(k)$ when $k = 1.5$. The reconstructed positive value of the source function is 1.09 (relative error 9.0%). The reconstructed negative value of the source function is -0.89 (relative error 11.0%).

are quite acceptable. Given that the noise in the data is 5%, errors in values of the function f^{comp} are also of an acceptable.

4. *Test 4. Problem 2. Ring.* We consider a model that is similar to that in the previous test. The main difference is the "outer positive" part of the true source function is a ring rather than a square. The function f_{true} is

$$f_{\text{true}} = \begin{cases} 1 & \text{if } 0.52^2 < x^2 + y^2 < 1.2^2, \\ -2 & \text{if } x^2 + y^2 \leq 0.52^2, \\ 0 & \text{otherwise,} \end{cases} \tag{3.4.16}$$

and $g_{\text{true}}(k) = k^2$ for all $k \in [\underline{k}, \overline{k}]$.

In Figure 3.5, one can see that the source function is computed rather accurately.

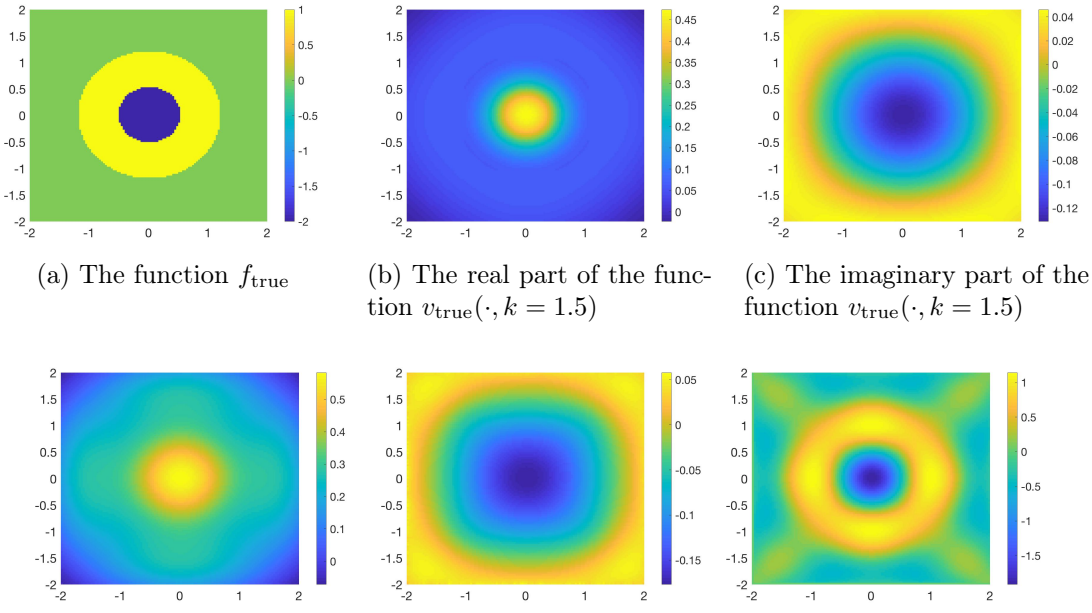

(a) The function f_{true}

(b) The real part of the function $v_{\text{true}}(\cdot, k = 1.5)$

(c) The imaginary part of the function $v_{\text{true}}(\cdot, k = 1.5)$

(d) The real part of the function $v_{\text{comp}}(\cdot, k = 1.5)$

(e) The imaginary part of the function $v_{\text{comp}}(\cdot, k = 1.5)$

(f) The function f_{comp}

Figure 3.5: Test 4. The true and reconstructed source functions and the true and reconstructed functions $v(\mathbf{x}, k) = u(\mathbf{x}, k)/g(k)$ when $k = 1.5$. The reconstructed positive value of the source function is 1.12 (relative error 12.0%). The reconstructed negative value of the source function is -1.94 (relative error 3.0%).

The values of both “positive" and “negative" parts of the inclusion are computed with a good accuracy.

5. *Test 5. 2. Continuous surface.* We take for $(x, y) \in \Omega$

$$f_{\text{true}} = 3(1-x)^2 e^{-x^2} - (y+1)^2 - 10(x/5 - x^3 - y^5)e^{-x^2-y^2} - 1/3e^{-(x+1)^2-y^2},$$

which is the function “peaks" built-in Matlab, restricted on Ω. This function is interesting since its support is not compactly contained in Ω and its graph behaves as a surface rather than the “inclusion" from the previous tests. We set $g_{\text{true}}(k) = \sin(k) + 2$ for all $k \in [\underline{k}, \overline{k}]$.

The numerical results for this test are displayed in Figure 3.6. It is evident that

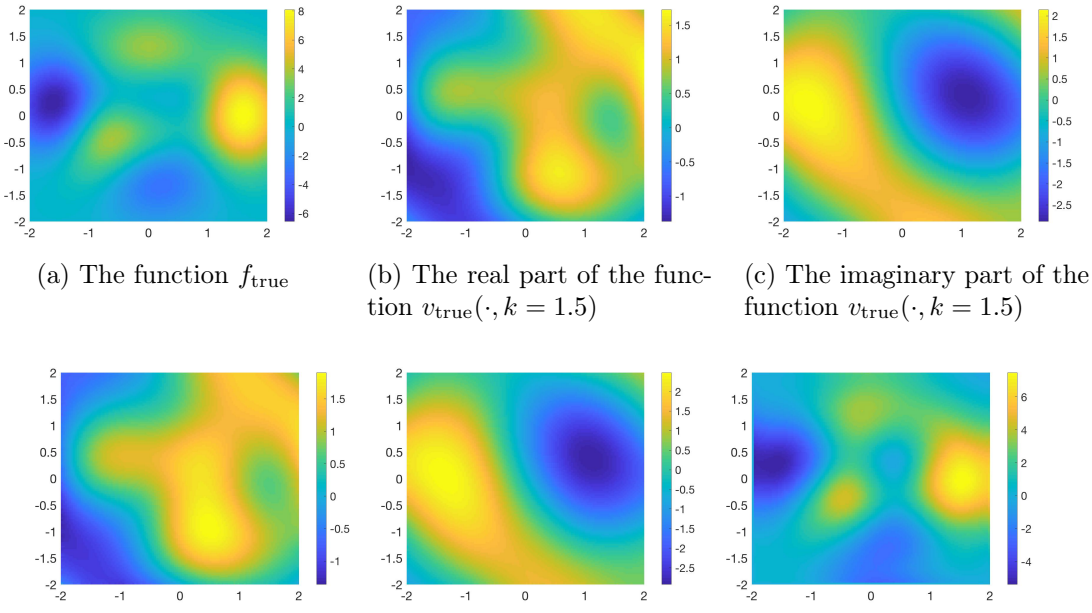

(a) The function f_{true}

(b) The real part of the function $v_{\text{true}}(\cdot, k = 1.5)$

(c) The imaginary part of the function $v_{\text{true}}(\cdot, k = 1.5)$

(d) The real part of the function $v_{\text{comp}}(\cdot, k = 1.5)$

(e) The imaginary part of the function $v_{\text{comp}}(\cdot, k = 1.5)$

(f) The function f_{comp}

Figure 3.6: Test 5. The true and reconstructed source functions and the true and reconstructed functions $v(\mathbf{x}, k) = u(\mathbf{x}, k)/g(k)$ when $k = 1.5$. The true and reconstructed maximal positive value of the source function are 8.10 and 7.36 (relative error 9.1%) respectively. The true and reconstructed minimal negative value of the source function are -6.55 and -5.48 (relative error 16.0%) respectively.

our method works well for this interesting case.

CHAPTER 4: PARABOLIC EQUATION

4.1 The algorithm

4.1.1 An orthonormal basis of $L^2(0,T)$ and the truncated Fourier series

We introduced an orthonormal basis of $L^2(a,b)$ in section 2.1. Now we set $a=0$ and $b=T$. Then

$$u(\mathbf{x},t)=\sum_{n=1}^{\infty}u_n(\mathbf{x})\Psi_n(t) \tag{4.1.1}$$

where

$$u_n(\mathbf{x})=\int_0^T u(\mathbf{x},t)\Psi_n(t)dt,\quad n=1,2,\ldots. \tag{4.1.2}$$

Fix a positive integer N. We truncate the Fourier series in (4.1.1). The function $u(\mathbf{x},t)$ is approximated by

$$u(\mathbf{x},t)=\sum_{n=1}^{N}u_n(\mathbf{x})\Psi_n(t)\quad \mathbf{x}\in\Omega, t\in[0,T]. \tag{4.1.3}$$

In this context, the partial derivative with respect to t of $u(\mathbf{x},t)$ is approximated by

$$u_t(\mathbf{x},t)=\sum_{n=1}^{N}u_n(\mathbf{x})\Psi_n'(t) \tag{4.1.4}$$

for all $\mathbf{x}\in\Omega$ and $t\in(0,T)$.

4.1.2 An approximate model

We introduce in this subsection a coupled system of elliptic partial differential equations without the presence of the unknown function $f(\mathbf{x})$. Plugging (4.1.3) and

(4.1.4) into (1.2.4), we have

$$\sum_{n=1}^{N} u_n(\mathbf{x})\Psi_n'(t) = \sum_{n=1}^{N} Lu_n(\mathbf{x})\Psi_n(t). \tag{4.1.5}$$

for all $\mathbf{x} \in \Omega$ and $t \in [0, T]$. For each $m \in \{1, \ldots, N\}$, multiply $\Psi_m(t)$ to both sides of (4.1.5) and then integrating the obtained equation with respect to t, we obtain

$$\sum_{n=1}^{N} \left(\int_0^T \Psi_m(t)\Psi_n'(t)dt \right) u_n(\mathbf{x}) = \sum_{n=1}^{N} \left(\int_0^T \Psi_m(t)\Psi_n(t)dt \right) Lu_n(\mathbf{x}) \tag{4.1.6}$$

for all $\mathbf{x}$ in Ω. Denote by

$$s_{mn} = \int_0^T \Psi_m(t)\Psi_n'(t)dt \tag{4.1.7}$$

and note that

$$\int_0^T \Psi_m(t)\Psi_n(t)dt = \begin{cases} 1 & \text{if } m = n, \\ 0 & \text{if } m \neq n. \end{cases} \tag{4.1.8}$$

We rewrite (4.1.6) as

$$\sum_{n=1}^{N} s_{mn}u_n(\mathbf{x}) = Lu_m(\mathbf{x}) \quad \mathbf{x} \in \Omega, m = 1, 2, \ldots, N. \tag{4.1.9}$$

Denote

$$U(\mathbf{x}) = (u_1(\mathbf{x}), u_2(\mathbf{x}), \ldots, u_N(\mathbf{x}))^T. \tag{4.1.10}$$

It follows from (4.1.9) that

$$LU(\mathbf{x}) = SU(\mathbf{x}) \quad \text{for } \mathbf{x} \in \Omega. \tag{4.1.11}$$

Here, the operator $\mathcal{L}$ acting on the vector $U(\mathbf{x})$ is understood in the same manner as it acts on scalar valued function, see (1.2.3).

On the other hand, due to (4.1.2) and (1.2.5), the vector $U(\mathbf{x})$ satisfies the boundary conditions

$$U(\mathbf{x}) = \widetilde{F}(\mathbf{x}) = \left(\int_0^T F(\mathbf{x},t)\Psi_1(t)dt, \ldots, \int_0^T F(\mathbf{x},t)\Psi_N(t)dt \right)^T \tag{4.1.12}$$

$$\partial_\nu U(\mathbf{x}) = \widetilde{G}(\mathbf{x}) = \left(\int_0^T G(\mathbf{x},t)\Psi_1(t)dt, \ldots, \int_0^T G(\mathbf{x},t)\Psi_N(t)dt \right)^T \tag{4.1.13}$$

for all $\mathbf{x} \in \partial\Omega$.

Remark 4.1.1. *From now on, we consider $\widetilde{F}$ and $\widetilde{G}$ as our "indirect" boundary data. This is acceptable since these two functions can be computed directly by the algebraic formulas* (4.1.12) *and* (4.1.13).

Finding a vector $U(\mathbf{x})$ satisfying equation (4.1.11) and constraints (4.1.12) and (4.1.13) is the main point in our numerical method to find the function $f(\mathbf{x})$. In fact, having $U(\mathbf{x}) = (u_1(\mathbf{x}), \ldots, u_2(\mathbf{x}), \ldots, u_N(\mathbf{x}))$ in hand, we can compute the function $u(\mathbf{x},t)$ via (4.1.3). The desired function $f(\mathbf{x})$ is given by $u(\mathbf{x}, t = 0)$.

Due to the truncation step in (4.1.3), equation (4.1.11) is not exact. We call it an *approximate model*. Solving it, together with the "over-determined" boundary conditions (4.1.12) and (4.1.13), for the Fourier coefficients $(u_n(\mathbf{x}))_{n=1}^N$ of $u(\mathbf{x},t)$, $\mathbf{x} \in \Omega$, $t \in [0,T]$, might not be rigorous. In fact, proving the "accuracy" of (4.1.11) when $N \to \infty$ is extremely challenging and is out of the scope of this dissertation. However, we experience in many earlier works that the solution of (4.1.11), (4.1.12) and (4.1.13) well approximates Fourier coefficients of the function $u(\mathbf{x},t)$, leading to good solutions of variety kinds of inverse problems, see [17, 18, 40, 41].

Remark 4.1.2 (The choice of N)**.** *On $\Omega = (-2,2)^2$, we arrange 81×81 grid points $\{(x_i, y_j) : 1 \le i, j \le 81\}$. In Figure 4.1 displays the functions of $u(\mathbf{x},t)$ and its approximation $\sum_{n=1}^N u_n(\mathbf{x})\Psi_n(t)$ where $u(\mathbf{x},t)$ is the true solution of the forward problem and $u_n(\mathbf{x})$, $n = 1, \ldots, N$, is computed using* (4.1.2). *This numerical experiment sug-*

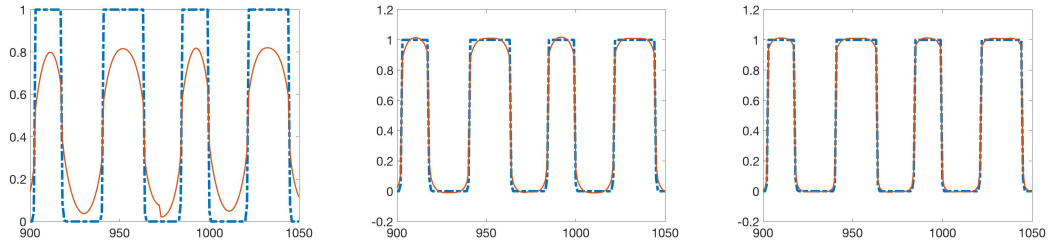

(a) $N = 10$ (b) $N = 20$ (c) $N = 30$

Figure 4.1: The function $u(\mathbf{x}, t = 0)$ (dash-dot) and its approximation $\sum_{n=1}^{N} u_n(\mathbf{x})\Psi_n(t = 0)$ (solid) at the points numbered from 900 to 1050. These functions are taken from Test 4 in Section 4.3.2. It is evident that the larger N, the better approximation for the function u is obtained by the N^{th} partial sum of the Fourier series in (4.1.1).

gests us to take $N = 30$. *It is worth mentioning that when* $N \leq 25$, *the numerical solutions are not satisfactory, when* $N = 30$, *numerical results are quite accurate regardless the high noise levels and when* $N \geq 35$, *the computation is time-consuming.*

4.1.3 The quasi-reversibility method

As mentioned, our method to solve Problem 3 is based on a numerical solver for (4.1.11), (4.1.12) and (4.1.13). We do so by employing the quasi-reversibility method; that means, we minimize the functional

$$J_\epsilon(U) = \int_\Omega |LU(\mathbf{x}) - SU(\mathbf{x})|^2 d\mathbf{x} + \epsilon \|U\|^2_{H^3(\Omega)}. \tag{4.1.14}$$

subject to the constraints (4.1.12) and (4.1.13). Here ϵ is a positive number serving as a regularization parameter. Impose the condition that the set of admissible data

$$H = \{V \in H^3(\Omega)^N : V|_{\partial\Omega\times[0,T]} = \widetilde{F} \text{ and } \partial V|_{\partial\Omega\times[0,T]} = \widetilde{G}\} \tag{4.1.15}$$

is nonempty, where $\widetilde{F}$ and $\widetilde{F}$ are our indirect data, see Remark 4.1.1, defined in (4.1.12) and (4.1.13). The result below guarantees the existence and uniqueness for the minimizer of J_ϵ, $\epsilon > 0$.

Proposition 4.1.1. *Assume that the set of admissible data H, defined in* (4.1.15)*, is nonempty. Then, for all $\epsilon > 0$, the functional J_ϵ admits a unique minimizer satisfying* (4.1.12) *and* (4.1.13)*. This minimizer is called the regularized solution to* (4.1.11)*,* (4.1.12) *and* (4.1.13)*.*

Proof. Proposition 4.1.1 is an analog of [40, Theorem 3.1] whose proof is based on the Riesz representation theorem. An alternative method to prove this proposition is from the standard argument in convex analysis, see e.g. [44, 47]. □

The minimizer of J_ϵ in H is called the *regularized solution* of (4.1.11), (4.1.12) and (4.1.13) obtained by the quasi-reversibility method.

The analysis above leads to Algorithm 3, which describes our numerical method to reconstruct the function $f(\mathbf{x})$, $\mathbf{x} \in \Omega$. In the next section, we establish a new Carleman estimate. This estimate plays an important role in proving the convergence of the regularized solution, due to the quasi-reversibility method, to the true solution of (4.1.11), (4.1.12) and (4.1.13) in Section 4.2 as the measurement noise and ϵ tend to 0.

Algorithm 3 The procedure to solve Problem 3

1: Choose a number N. Construct the functions Ψ_m, $1 \leq m \leq N$, in Section 2.1 and compute the matrix S whose the mn^{th} entry is given in 4.1.7.
2: Calculate the boundary data $\widetilde{F}$ and $\widetilde{G}$ for the vector valued function U via (4.1.12) and (4.1.13) respectively.
3: Solve (4.1.11), (4.1.12)) and (4.1.13) via the quasi-reversibility method for the vector
$$U(\mathbf{x}) = (u_1(\mathbf{x}), \dots, u_N(\mathbf{x}))^T \quad \mathbf{x} \in \Omega.$$
4: Compute $u(\mathbf{x}, t)$, $(\mathbf{x}, t) \in \Omega \times [0, T]$ using (4.1.1).
5: Set the desired function $f(\mathbf{x}) = u(\mathbf{x}, 0)$ for all $\mathbf{x} \in \Omega$.

4.2 Convergence Analysis

In this section, we continue to assume (2.2.37). Let $\widetilde{F}^*$ and $\widetilde{G}^*$ be the noiseless data for (4.1.12) and (4.1.13), see Remark (4.1.1), respectively. The noisy data are denoted by $\widetilde{F}^\delta$ and $\widetilde{G}^\delta$. Here δ is the noise level. In this section, assume that there exists $\mathcal{E} \in H^3(\Omega)^N$ such that

1. for all $\mathbf{x} \in \Omega$

$$\mathcal{E}(\mathbf{x}) = \widetilde{F}^\delta(\mathbf{x}) - \widetilde{F}^*(\mathbf{x}) \quad \text{and} \quad A(\mathbf{x})\nabla\mathcal{E}(\mathbf{x}) \cdot \nu(\mathbf{x}) = \widetilde{G}^\delta(\mathbf{x}) - \widetilde{G}^*(\mathbf{x}); \quad (4.2.1)$$

2. and the bound

$$\|\mathcal{E}\|_{H^3(\Omega)^N} < \delta \quad \text{as } \delta \to 0^+ \quad (4.2.2)$$

holds true.

The assumption about the existence of $\mathcal{E}$ satisfying (4.2.1) and (4.2.2) is equivalent to the condition

$$\inf\{\|\Phi\|_{H^3(\Omega)^N} : \Phi|_{\partial\Omega} = \widetilde{F}^\delta - \widetilde{F}^*, \partial_\nu\Phi|_{\partial\Omega} = \widetilde{G}^\delta - \widetilde{G}^*\} < \delta.$$

In this section, we establish the following result to study the accuracy of the quasi-reversibility method.

Theorem 4.2.1. *Assume that U^* is the function that satisfies* (3.1.10), (3.1.13) *and* (3.1.14) *with $\widetilde{F}$ and $\widetilde{G}$ replaced by $\widetilde{F}^*$ and $\widetilde{G}^*$ respectively. Fix $\epsilon > 0$. Let U^δ be the minimizer of J_ϵ subject to constraints* (3.1.13) *and* (3.1.14) *with $\widetilde{F}$ and $\widetilde{G}$ replaced by $\widetilde{F}^\delta$ and $\widetilde{G}^\delta$ respectively. Assume further that there is an "error" function $\mathcal{E}$ in $H^3(\Omega)^N$ satisfying* (4.2.1) *and* (4.2.2). *Then, we have the estimate*

$$\|U^\delta - U^*\|^2_{H^3(\Omega)^N} \leq C\left(\delta^2 + \epsilon\|U^*\|^2_{H^3(\Omega)^N}\right) \quad (4.2.3)$$

where C is a constant that depends only on Ω, $\|A\|_{C^1(\overline{\Omega})}$ and μ.

Proof. Since U^δ is the minimizer of J_ϵ, by the variational principle, we have

$$\langle LU^\delta - SU^\delta, L\Phi - S\Phi\rangle_{L^2(\Omega)^N} + \epsilon\langle U^\delta, \Phi\rangle_{H^3(\Omega)^N} = 0 \tag{4.2.4}$$

for all test functions Φ in the space

$$H_0^3(\Omega)^N = \{\phi \in H^3(\Omega)^N : \phi = A\nabla\phi \cdot \nu = 0 \text{ on } \partial\Omega\}.$$

Since $LU^* - SU^* = 0$, we can deduce from (4.2.4) that

$$\langle L(U^\delta - U^*) - S(U^\delta - U^*), L\Phi - S\Phi\rangle_{L^2(\Omega)^N} + \epsilon\langle U^\delta - U^*, \Phi\rangle_{H^3(\Omega)^N} = -\epsilon\langle U^*, \Phi\rangle_{H^3(\Omega)^N}.$$

Plugging the test function

$$\Phi = U^\delta - U^* - \mathcal{E} \in H_0^3(\Omega) \tag{4.2.5}$$

into the identity above, we have

$$\begin{aligned}\|L\Phi - S\Phi\|^2_{L^2(\Omega)^N} + \epsilon\|\Phi\|^2_{H^3(\Omega)^N} = &-\langle L\mathcal{E} - S\mathcal{E}, L\Phi - S\Phi\rangle^2_{L^2(\Omega)^N} \\ &- \epsilon\langle\mathcal{E}, \Phi\rangle_{H^3(\Omega)^N} - \epsilon\langle U^*, \Phi\rangle_{H^3(\Omega)^N}.\end{aligned}$$

Applying the Cauchy–Schwartz inequality and removing lower order terms, we obtain

$$\|L\Phi - S\Phi\|^2_{L^2(\Omega)^N} + \epsilon\|\Phi\|^2_{H^3(\Omega)^N} \leq C\left(\delta^2 + \epsilon\|U^*\|^2_{H^3(\Omega)^N}\right). \tag{4.2.6}$$

Recall from (1.2.3) that

$$\|L\Phi - S\Phi\|^2_{L^2(\Omega)^N} = \|\mathrm{Div}(A(\mathbf{x})\nabla\Phi + \mathbf{b}(\mathbf{x}) \cdot \nabla\Phi + (c(\mathbf{x})\mathrm{Id} - S)\Phi\|^2_{L^2(\Omega)^N}$$

Recall the function ψ in (2.2.38). Fix $\lambda > \sigma_0$ and $p > \sigma_1$ as in Lemma 2.2.1. Set

$$M = \max\{e^{2\lambda\psi^{-p}(\mathbf{x})} : \mathbf{x} \in \overline{\Omega}\} \quad \text{and} \quad m = \min\{e^{2\lambda\psi^{-p}(\mathbf{x})} : \mathbf{x} \in \overline{\Omega}\}.$$

We have

$$M\|L\Phi - S\Phi\|^2_{L^2(\Omega)^N} \geq \frac{1}{2}\big\|e^{\lambda\psi^{-p}(\mathbf{x})}\mathrm{Div}(A(\mathbf{x})\nabla\Phi) + e^{\lambda\psi^{-p}(\mathbf{x})}(\mathbf{b}(\mathbf{x})\cdot\nabla\Phi + (c(\mathbf{x})\mathrm{Id} - S)\Phi)\big\|^2_{L^2(\Omega)^N}.$$

Using the inequality $(x-y)^2 \geq \frac{1}{2}x^2 - y^2$, we have

$$M\|L\Phi - S\Phi\|^2_{L^2(\Omega)^N} \geq \frac{1}{2}\|e^{\lambda\psi^{-p}(\mathbf{x})}\mathrm{Div}(A(\mathbf{x})\nabla\Phi)\|^2_{L^2(\Omega)^N} - \|e^{\lambda\psi^{-p}(\mathbf{x})}(\mathbf{b}(\mathbf{x})\cdot\nabla\Phi + (c(\mathbf{x})\mathrm{Id} - S)\Phi)\|^2_{L^2(\Omega)^N}.$$

Thus, by (2.2.42),

$$M|L\Phi - S\Phi\|^2_{L^2(\Omega)^N} \geq Cm\|\Phi\|_{H^1(\Omega)^N} \tag{4.2.7}$$

Combining (4.2.5), (4.2.6) and (4.2.7) gives

$$\|U^\delta - U^* - \mathcal{E}\|^2_{H^1(\Omega)^N} \leq C\left(\delta^2 + \epsilon\|U^*\|^2_{H^3(\Omega)^N}\right).$$

This and the assumption $\|\mathcal{E}\|_{H^3(\Omega)^N} \leq C\delta$ imply inequality (4.2.3). □

Corollary 4.2.1. *Let $f^*(\mathbf{x}) = u^*(\mathbf{x}, 0)$ and $f^\delta(\mathbf{x}) = u^\delta(\mathbf{x}, 0)$ where $u^*(\mathbf{x}, t)$ and $u^\delta(\mathbf{x}, t)$ are computed from $U^*(\mathbf{x})$ and $U^\delta(\mathbf{x})$ via (4.1.1) and (4.1.10). Then, by the trace theory*

$$\|f^\delta - f^*\|_{L^2(\Omega)} \leq C\left(\delta + \sqrt{\epsilon}\|U^*\|_{H^3(\Omega)^N}\right).$$

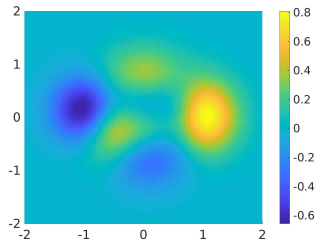

Figure 4.2: The true function $c(\mathbf{x})$ used for all numerical examples in this section.

4.3 Numerical illustrations

We numerically test our method when $d = 2$. The domain Ω is the square $(-R, R)^2$. In this section, we write $\mathbf{x} = (x, y)$. For the coefficients of the governing equation, we choose, for simplicity, $A(\mathbf{x}) = \mathrm{Id}$ and $\mathbf{b}(\mathbf{x}) = 0$. The function c is set as

$$c(x, y) = (3(1 - x)^2 e^{-x^2-(y+1)^2} - 10(x/5 - x^3 - y^5)e^{-x^2-y^2} - 1/3e^{-(x+1)^2-y^2})/10$$

which is a scale of the "peaks" function in Matlab. The graph of c is displayed in Figure 4.2.

Define a grid of points in Ω

$$\mathcal{G} = \{(x_i, y_j) = (-R + (i - 1)d_{\mathbf{x}}, -R + (j - 1)d\mathbf{x}) : 1 \leq i, j \leq N_{\mathbf{x}} + 1\}$$

where $N_{\mathbf{x}} = 80$ and $d_{\mathbf{x}} = 2R/N_{\mathbf{x}}$. For the time variable, we choose $T = 4$. Define a uniform partition of $[0, T]$ as

$$0 = t_1 < t_2 < \cdots < t_{N_T+1} = T$$

with step size $d_t = T/N_T$. In our tests, $N_T = 250$. The forward problem is solved by finite difference method in the implicit scheme. Denote by u^* the solution of the

forward problem. The data is given by

$$F(\mathbf{x},t) = u(\mathbf{x},t)(1+\delta(2\text{rand}-1)) \quad G(\mathbf{x},t) = \partial_\nu u(\mathbf{x},t)(1+\delta(2\text{rand}-1))$$

for $(\mathbf{x},t) \in \partial\Omega \times [0,T]$ where rand is the uniformly distributed random function taking value in $[0,1]$ and δ is the noise level. The noise level δ is given in each numerical tests.

4.3.1 The implementation for Algorithm 3

The main part of this section is to compute the minimizer U of J_ϵ subject to the constraints (3.1.13) and (3.1.14). The "cut-off" number N is set to be 30, see Remark 4.1.2 for this choice of N. The discretized version of $U(\mathbf{x}) = (u_1(\mathbf{x}), \ldots, u_N(\mathbf{x}))^T$, $\mathbf{x} \in \Omega$ is $(u_1(x_i,y_j), \ldots, u_N(x_i,y_j))_{i,j=1}^{N_\mathbf{x}+1}$. Hence, $J_\epsilon(U)$, see (4.1.14), is approximated by

$$\begin{aligned} &J_\epsilon(U) = \\ &d_\mathbf{x}^2 \sum_{i,i=2}^{N_\mathbf{x}} \sum_{m=1}^{N} \Big| \frac{u_m(x_{i+1},y_j) + u_m(x_{i-1},y_j) + u_m(x_i,y_{j+1}) + u_m(x_i,y_{j-1}) - 4u_m(x_i,y_j)}{d_\mathbf{x}^2} \\ &\qquad + c(x_i,y_j)u_m(x_i,y_j) + \sum_{n=1}^{N} s_{mn}u_n(x_i,y_j) \Big|^2 + \epsilon d_\mathbf{x}^2 \sum_{i,j=2}^{N_x} \sum_{m=1}^{N} |u_m(x_i,y_j)|^2 \\ &+\epsilon^2 d_\mathbf{x}^2 \sum_{i,j=2}^{N_\mathbf{x}} \sum_{m=1}^{N} \Big| \frac{u_m(x_{i+1},y_j) - u_m(x_i,y_j)}{d_\mathbf{x}} \Big|^2 + \epsilon^2 d_\mathbf{x}^2 \sum_{i,j=2}^{N_\mathbf{x}} \sum_{m=1}^{N} \Big| \frac{u_m(x_i,y_{j+1}) - u_m(x_i,y_j)}{d_\mathbf{x}} \Big|^2. \end{aligned} \tag{4.3.1}$$

Here, we slightly change the H^3 norm of the regularity term to the H^1 norm. This makes the computational codes less heavy. The numerical results with this change are still acceptable. We also modify the regularized parameter of the term $\|\nabla U\|_{L^2(\Omega)^N}$ to be ϵ^2, instead of ϵ, since we observe that the obtained numerical results are more

accurate with this modification. The expression in (4.3.1) is simplified as follows

$$J_\epsilon(U) = d_{\mathbf{x}}^2 \sum_{i,j=2}^{N_x} \sum_{m=1}^{N} \Big| \sum_{n=1}^{N} \left[\delta_{mn} \left(\frac{-4}{d_{\mathbf{x}}^2} + c(x_i, y_j) \right) - s_{mn} \right] u_n(x_i, y_j) + \frac{\delta_{mn}}{d_{\mathbf{x}}^2} u_n(x_{i+1}, y_j)$$
$$+ \frac{\delta_{mn}}{d_{\mathbf{x}}^2} u_n(x_{i-1}, y_j) + \frac{\delta_{mn}}{d_{\mathbf{x}}^2} u_n(x_i, y_{j+1}) + \frac{\delta_{mn}}{d_{\mathbf{x}}^2} u_n(x_i, y_{j-1}) \Big|^2 + \epsilon d_{\mathbf{x}}^2 \sum_{i,j=2}^{N_x} \sum_{m=1}^{N} |u_m(x_i, y_j)|^2$$
$$+\epsilon^2 d_{\mathbf{x}}^2 \sum_{i,j=2}^{N_{\mathbf{x}}} \sum_{m=1}^{N} \left| \frac{u_m(x_{i+1}, y_j) - u_m(x_i, y_j)}{d_{\mathbf{x}}} \right|^2 + \epsilon^2 d_{\mathbf{x}}^2 \sum_{i,j=2}^{N_{\mathbf{x}}} \sum_{m=1}^{N} \left| \frac{u_m(x_i, y_{j+1}) - u_m(x_i, y_j)}{d_{\mathbf{x}}} \right|^2. \tag{4.3.2}$$

Here, we use the Kronecker number δ_{mn} for the convience of writing the computational codes. We next identify $\{u_n(x_i, y_j) : 1 \le i, j \le N_{\mathbf{x}} + 1, 1 \le n \le N\}$ with the $(N_{\mathbf{x}} + 1)^2 N$ dimensional vector $\mathfrak{U} = (\mathfrak{u}_{\mathfrak{i}})_{\mathfrak{i}=1}^{(N_{\mathbf{x}}+1)^2 N}$ according to the rule $\mathfrak{u}_{\mathfrak{i}} = u_n(x_i, y_j)$ where the index $\mathfrak{i}$ is

$$\mathfrak{i} = (i-1)(N_{\mathbf{x}} + 1)N + (j-1)N + n, \quad 1 \le i, j \le N_{\mathbf{x}} + 1, 1 \le n \le N.$$

Then, with this notation, $J_\epsilon(U)$ in (4.3.2) is rewritten as

$$\mathfrak{J}_\epsilon(\mathfrak{U}) = d_{\mathbf{x}}^2 |\mathfrak{L}\mathfrak{U}|^2 + + \epsilon d_{\mathbf{x}}^2 |\mathfrak{U}|^2 + \epsilon d_{\mathbf{x}}^2 |D_x \mathfrak{U}|^2 + \epsilon d_{\mathbf{x}}^2 |D_y \mathfrak{U}|^2.$$

The $(N_{\mathbf{x}} + 1)^2 N \times (N_{\mathbf{x}} + 1)^2 N$ matrices $\mathfrak{L}$, D_x and D_y are as follows.

1. *Define the matrix* $\mathfrak{L}$. For $\mathfrak{i} = (i-1)(N_{\mathbf{x}} + 1)N + (j-1)N + m$, for some $2 \le i, j \le N_x$, the $\mathfrak{ij}^{\text{th}}$ entry of $\mathfrak{L}$ is

   (a) $\delta_{mn} \left(-4/d_{\mathbf{x}}^2 + c(x_i, y_j)\right) - s_{mn}$ if $\mathfrak{j} = (i-1)(N_{\mathbf{x}} + 1)N + (j-1)N + n$,

   (b) δ_{mn}/d_x^2 if $\mathfrak{j} = (i \pm 1 - 1)(N_{\mathbf{x}} + 1)N + (j-1)N + n$ or $\mathfrak{j} = (i-1)(N_{\mathbf{x}} + 1)N + (j \pm 1 - 1)N + n$,

   (c) 0 otherwise.

2. *Define the matrix* D_x. For $\mathfrak{i} = (i-1)(N_{\mathbf{x}}+1)N + (j-1)N + m$, for some $2 \le i, j \le N_x$, the $\mathfrak{ij}^{\text{th}}$ entry of D_x is

   (a) $1/d_{\mathbf{x}}$ if $\mathfrak{j} = (i+1-1)(N_{\mathbf{x}}+1)N + (j-1)N + m$,

   (b) $-1/d_{\mathbf{x}}$ if $\mathfrak{j} = \mathfrak{i}$,

   (c) 0 otherwise.

3. *Define the matrix* D_x. For $\mathfrak{i} = (i-1)(N_{\mathbf{x}}+1)N + (j-1)N + m$, for some $2 \le i, j \le N_x$, the $\mathfrak{ij}^{\text{th}}$ entry of D_x is

   (a) $1/d_{\mathbf{x}}$ if $\mathfrak{j} = (i-1)(N_{\mathbf{x}}+1)N + (j+1-1)N + m$,

   (b) $-1/d_{\mathbf{x}}$ if $\mathfrak{j} = \mathfrak{i}$,

   (c) 0 otherwise.

Remark 4.3.1 (The values of the parameters)**.** *As mentioned, we take* $N = 30$*,* $N_{\mathbf{x}} = 80$*,* $N_T = 250$*,* $R = 2$*. The regularized parameter* $\epsilon = 10^{-7}$*. These values of parameters are used for all tests in Section 4.3.2.*

4.3.2 Tests

We perform four (4) numerical examples in this dissertation. These examples with high levels of noise show the strength of our method. We will also compare the reconstructed maximum values of the reconstructed functions and the true ones. Below, f_{true} and f_{comp} are, respectively, the true source function and the reconstructed one due to Algorithm 3 with the parameters in Section 4.3.1.

1. *Test 1. The case of one inclusion.* The function f_{true} is a smooth function supported in a disk with radius 1 centered at the origin. More precisely,

$$f_{\text{true}}(\mathbf{x}) = \begin{cases} e^{-\frac{1}{1-|\mathbf{x}|^2}+1} & \text{if } |\mathbf{x}| < 1, \\ 0 & \text{otherwise.} \end{cases}$$

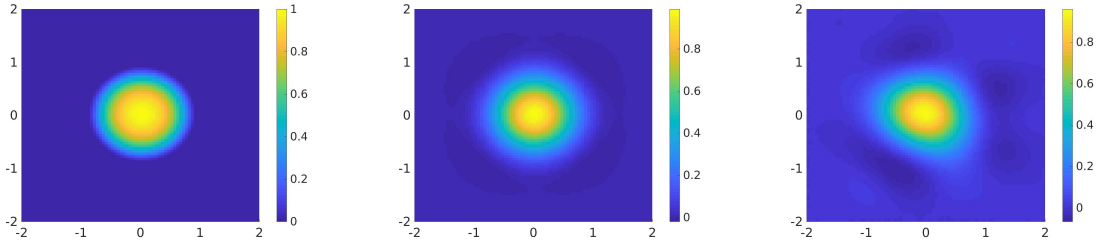

(a) The function f_{true} (b) f_{comp}, $\delta = 0\%$ (c) f_{comp}, $\delta = 25\%$

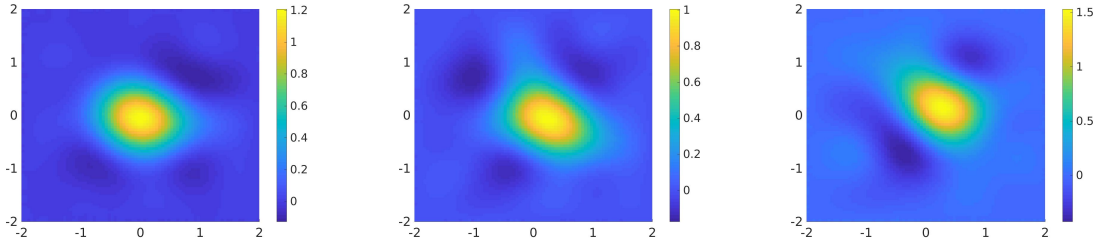

(d) f_{comp}, $\delta = 50\%$ (e) f_{comp}, $\delta = 75\%$ (f) f_{comp}, $\delta = 100\%$

Figure 4.3: Test 1. The true and computed source functions. Our method still works well when $\delta = 100\%$. It is shown in (e) that the reconstructed value of f_{comp} with $\delta = 75\%$ is quite accurate, even better than in (d), but in contrast, the reconstructed shape starts to break down.

Figure 4.3 displays the functions f_{true} and f_{comp}. Table 4.1 show the reconstructed value of the function f_{comp} and the relative error. The noise levels are $\delta = 0\%$, 25%, 50%, 75% and 100%.

It is evident that our method is robust for Test 1 in the sense that the reconstructed maximal value of the function f and the reconstructed shape and position of the inclusion are quite accurate.

2. *Test 2. The case of two inclusions.* The function f_{true} is a smooth function supported in two disks with radius $r = 0.8$ centered at $\mathbf{x}_1 = (-1, 0)$ and $\mathbf{x}_2 =$

Table 4.1: Test 1. Correct and computed maximal values of source functions. $\text{error}_{\text{rel}}$ denotes the relative error of the reconstructed maximal value. pos_{true} is the true position of the inclusion; i.e., the maximizer of f_{true}. pos_{comp} is the computed position of the inclusion. dis_{err} is the absolute error of the reconstructed positions.

noise level	$\max f_{\text{true}}$	$\max f_{\text{comp}}$	$\text{error}_{\text{rel}}$	pos_{true}	pos_{comp}	dis_{err}
0%	1	0.99	1.0%	$(0,0)$	$(0,0)$	0
25%	1	0.96	4.0%	$(0,0)$	$(-0.05,0)$	0.05
50%	1	1.21	21.0%	$(0,0)$	$(-0.05,0.1)$	0.11
75%	1	1.01	1.0%	$(0,0)$	$(0.2,-0.1)$	0.22
100%	1	1.53	53.0%	$(0,0)$	$(0.25,0.1)$	0.27

$(1,0)$ respectively. The function f_{true} is given by the formula

$$f(\mathbf{x}) = \begin{cases} e^{-\frac{r^2}{r^2-|\mathbf{x}-\mathbf{x}_1|^2}+1} & \text{if } |\mathbf{x}-\mathbf{x}_1| < r, \\ e^{-\frac{r^2}{r^2-|\mathbf{x}-\mathbf{x}_2|^2}+1} & \text{if } |\mathbf{x}-\mathbf{x}_2| < r, \\ 0 & \text{otherwise.} \end{cases}$$

Figure 4.4 displays the functions f_{true} and f_{comp}. Table 4.2 show the reconstructed value of the function f_{comp} and the relative error. The noise levels are $\delta = 0\%$, 25%, 50%, 75% and 100%.

The reconstruction in Test 2 is good. In this test, the reconstruct breaks down when the noise level is 75% although we are able to detect the inclusions with higher noise levels.

3. *Test 3. The case of non-inclusion and nonsmooth function.* The function f_{true} is the characteristic function of the letter Y. Figure 4.5 displays the functions f_{true} and f_{comp}. The noise levels are $\delta = 10\%$ and 15%.

   We can reconstruct the letter Y and the reconstructed maximal of f_{comp} is good when $\delta = 10\%$ but the error is large when the noise level reaches 15%.

4. *Test 4. The case of non-inclusion and nonsmooth function.* The function f_{true}

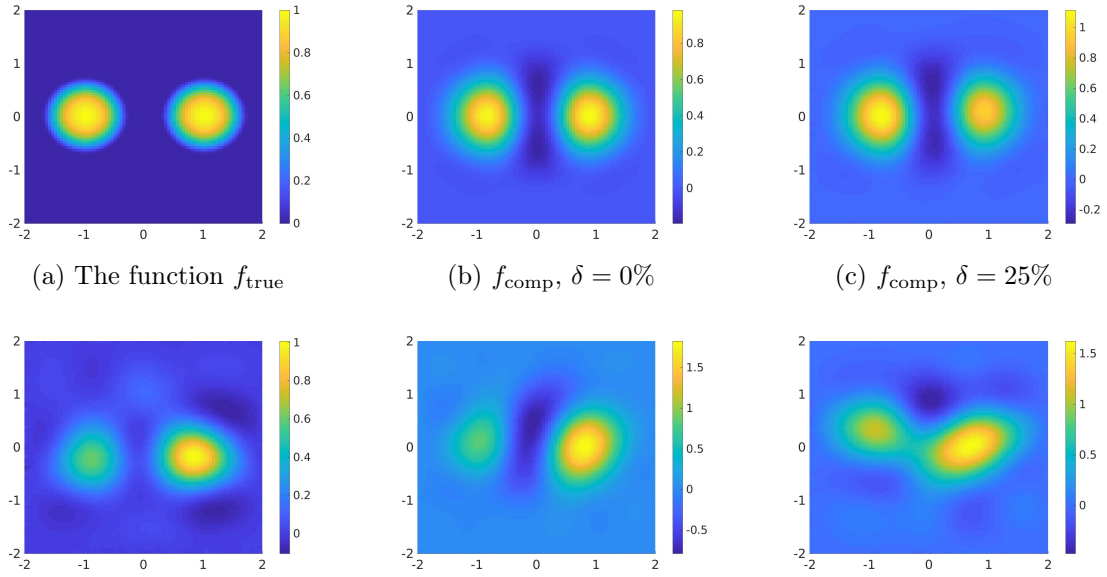

(a) The function f_{true} (b) f_{comp}, $\delta = 0\%$ (c) f_{comp}, $\delta = 25\%$

(d) f_{comp}, $\delta = 50\%$ (e) f_{comp}, $\delta = 75\%$ (f) f_{comp}, $\delta = 100\%$

Figure 4.4: Test 2. The true and computed source functions. The reconstruction of the two inclusions are not symmetric probably because the true function c, see Figure 4.2 for its graph, is negative on the left and positive on the right. However, both inclusions can be seen when the noise level goes up to 100%.

Table 4.2: Test 2. Correct and computed maximal values of the inclusions. $\max_{\text{inc,true}}$ and $\max_{\text{inc,comp}}$ are the true and computed, respectively, maximal values of the source in an inclusion. $\text{error}_{\text{rel}}$ denotes the relative error of the reconstructed maximal value. pos_{true} is the true position of the inclusion; i.e., the maximizer of f_{true}. pos_{comp} is the computed position of the inclusion. dis_{err} is the absolute error of the reconstructed positions.

noise level	inclusion	$\max_{\text{inc,true}}$	$\max_{\text{inc,comp}}$	$\text{error}_{\text{rel}}$	pos_{true}	pos_{comp}	dis_{err}
0%	left	1	0.96	4.0%	$(-1, 0)$	$(-0.85, 0)$	0.15
0%	right	1	0.98	2.0%	$(1, 0)$	$(0.85, 0)$	0.15
25%	left	1	1.11	11%	$(-1, 0)$	$(-0.85, 0)$	0.15
25%	right	1	0.96	4%	$(1, 0)$	$(0.9, 0.1)$	0.14
50%	left	1	0.61	39%	$(-1, 0)$	$(-0.9, 0.25)$	0.27
50%	right	1	1.01	1%	$(1, 0)$	$(0.85, -0.2)$	0.25
75%	left	1	0.84	26%	$(-1, 0)$	$(-1, 0.1)$	0.1
75%	right	1	1.82	82%	$(1, 0)$	$(0.8, 0)$	0.2
100%	left	1	1.1	10%	$(-1, 0)$	$(-0.9, 0.3)$	0.32
100%	right	1	1.58	58%	$(1, 0)$	$(0.05, 0.8)$	0.21

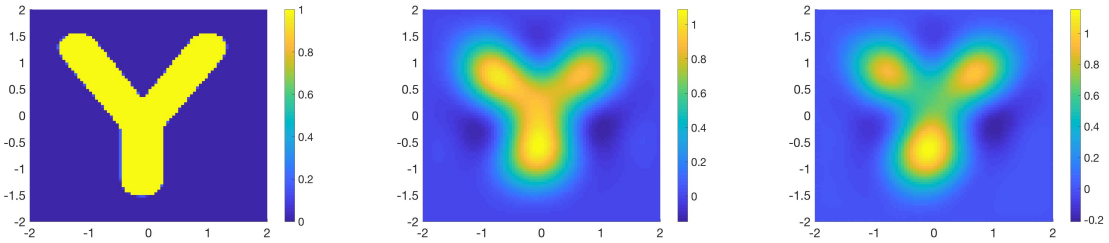

(a) The function f_{true} (b) f_{comp}, $\delta = 10\%$ (c) f_{comp}, $\delta = 15\%$

Figure 4.5: Test 3. The true and computed source functions. The letter Y can be detected well in this case. The true maximal value of f_{true} is 1. The computed maximal value of f_{comp} when $\delta = 10\%$ is 1.09 (relative error 9%). The computed maximal value of f_{comp} when $\delta = 15\%$ is 1.15 (relative error 15%).

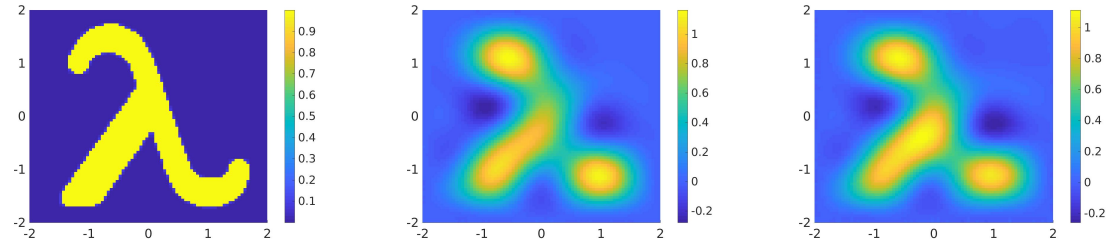

(a) The function f_{true} (b) f_{comp}, $\delta = 10\%$ (c) f_{comp}, $\delta = 15\%$

Figure 4.6: Test 4. The true and computed source functions. The reconstruction of λ is acceptable. The true maximal value of f_{true} is 1. The computed maximal value of f_{comp} when $\delta = 10\%$ is 1.16 (relative error 16%). The computed maximal value of f_{comp} when $\delta = 15\%$ is 1.11 (relative error 11%).

is the characteristic function of the letter λ. Figure 4.6 displays the functions f_{true} and f_{comp}. The noise levels are $\delta = 10\%$ and 15%.

The image of λ in Test 4 is acceptable. The reconstructed maximal value in Figure 4.6c is better than that in Figure 4.6b but the reconstruction of λ in Figure 4.6c is not as good as that in Figure 4.6b.

CHAPTER 5: CONCLUDING REMARKS

The main aim of this thesis is to solve two inverse source problems in the frequency domain. In this work, we derived a system of PDEs whose solutions directly provide the solution of the inverse source problems under consideration.

The main points of the method is derive approximate models by a truncation of the Fourier series with respect to a special basis. We solved the approximation models by the quasi-reversibility method. The convergence of this method when the noise tends to 0 was proved. More importantly, numerical examples show that our method is robust when proving accurate reconstructions of the unknown source function from highly noisy data.

REFERENCES

[1] G. Bao, J. Lin, and F. Triki, "A multi-frequency inverse source problem," *Journal of Differential Equations*, vol. 249, no. 12, pp. 3443–3465, 2010.

[2] G. Bao, J. Lin, F. Triki, *et al.*, "Numerical solution of the inverse source problem for the helmholtz equation with multiple frequency data," *Contemp. Math*, vol. 548, pp. 45–60, 2011.

[3] J. Cheng, V. Isakov, and S. Lu, "Increasing stability in the inverse source problem with many frequencies," *Journal of Differential Equations*, vol. 260, no. 5, pp. 4786–4804, 2016.

[4] A. El Badia and T. Ha-Duong, "An inverse source problem in potential analysis," *Inverse Problems*, vol. 16, no. 3, p. 651, 2000.

[5] G. Dassios and F. Kariotou, "Magnetoencephalography in ellipsoidal geometry," *Journal of Mathematical Physics*, vol. 44, no. 1, pp. 220–241, 2003.

[6] V. Isakov and S. Lu, "Increasing stability in the inverse source problem with attenuation and many frequencies," *SIAM Journal on Applied Mathematics*, vol. 78, no. 1, pp. 1–18, 2018.

[7] M. N. Entekhabi and V. Isakov, "On increasing stability in the two dimensional inverse source scattering problem with many frequencies," *Inverse Problems*, vol. 34, no. 5, p. 055005, 2018.

[8] V. Isakov and S. Lu, "Inverse source problems without (pseudo) convexity assumptions.," *Inverse Problems & Imaging*, vol. 12, no. 4, 2018.

[9] G. Bao, J. Lin, and F. Triki, "An inverse source problem with multiple frequency data," *Comptes Rendus Mathematique*, vol. 349, no. 15-16, pp. 855–859, 2011.

[10] X. Wang, Y. Guo, D. Zhang, and H. Liu, "Fourier method for recovering acoustic sources from multi-frequency far-field data," *Inverse Problems*, vol. 33, no. 3, p. 035001, 2017.

[11] M. V. Klibanov, "Estimates of initial conditions of parabolic equations and inequalities via lateral cauchy data," *Inverse problems*, vol. 22, no. 2, p. 495, 2006.

[12] A. El Badia and T. Ha-Duong, "On an inverse source problem for the heat equation. application to a pollution detection problem," *Journal of inverse and ill-posed problems*, vol. 10, no. 6, pp. 585–599, 2002.

[13] J. Li, M. Yamamoto, and J. Zou, "Conditional stability and numerical reconstruction of initial temperature," *Communications on Pure & Applied Analysis*, vol. 8, no. 1, pp. 361–382, 2009.

[14] M. M. Lavrent_ev, V. G. Romanov, and S. P. Shishatski_, *Ill-posed problems of mathematical physics and analysis. Translations of Mathematical Monographs.*, vol. 64. American Mathematical Soc., 1986.

[15] D. Colton and R. Kress, *Inverse acoustic and electromagnetic scattering theory*, vol. 93. Springer Science & Business Media, 2012.

[16] M. V. Klibanov, "Convexification of restricted dirichlet-to-neumann map," *Journal of Inverse and Ill-posed Problems*, vol. 25, no. 5, pp. 669–685, 2017.

[17] M. V. Klibanov and L. H. Nguyen, "Pde-based numerical method for a limited angle x-ray tomography," *arXiv preprint arXiv:1809.06012*, 2018.

[18] M. V. Klibanov, A. E. Kolesov, A. Sullivan, and L. Nguyen, "A new version of the convexification method for a 1d coefficient inverse problem with experimental data," *Inverse Problems*, vol. 34, p. 115014, sep 2018.

[19] A. Buchgeim and M. V. Klibanov, "Uniqueness in the large of a class of multidimensional inverse problems," in *Sov. Math. Dokl.*, vol. 24, pp. 244–247, 1981.

[20] L. Beilina and M. V. Klibanov, *Approximate global convergence and adaptivity for coefficient inverse problems*. Springer Science & Business Media, 2012.

[21] M. Bellassoued and M. Yamamoto, *Carleman estimates and applications to inverse problems for hyperbolic systems*. Springer, 2017.

[22] M. V. Klibanov and A. A. Timonov, *Carleman estimates for coefficient inverse problems and numerical applications*, vol. 46. Walter de Gruyter, 2012.

[23] M. V. Klibanov, "Carleman estimates for global uniqueness, stability and numerical methods for coefficient inverse problems," *Journal of Inverse and Ill-Posed Problems*, vol. 21, no. 4, pp. 477–560, 2013.

[24] M. V. Klibanov, J. Li, and W. Zhang, "Electrical impedance tomography with restricted dirichlet-to-neumann map data," *arXiv preprint arXiv:1803.11193*, 2018.

[25] M. V. Klibanov and N. T. Thanh, "Recovering dielectric constants of explosives via a globally strictly convex cost functional," *SIAM Journal on Applied Mathematics*, vol. 75, no. 2, pp. 518–537, 2015.

[26] S. I. Kabanikhin and M. A. Shishlenin, "Numerical algorithm for two-dimensional inverse acoustic problem based on gel'fand–levitan–krein equation," *Journal of Inverse and Ill-Posed Problems*, vol. 18, no. 9, pp. 979–995, 2011.

[27] S. I. Kabanikhin, A. D. Satybaev, and M. A. Shishlenin, *Direct methods of solving multidimensional inverse hyperbolic problems*, vol. 48. Walter de Gruyter, 2013.

[28] S. I. Kabanikhin, K. K. Sabelfeld, N. S. Novikov, and M. A. Shishlenin, "Numerical solution of the multidimensional gelfand–levitan equation," *Journal of Inverse and Ill-Posed Problems*, vol. 23, no. 5, pp. 439–450, 2015.

[29] R. Lattès and J.-L. Lions, "The method of quasi-reversibility: applications to partial differential equations," tech. rep., 1969.

[30] E. Bécache, L. Bourgeois, L. Franceschini, and J. Dardé, "Application of mixed formulations of quasi-reversibility to solve ill-posed problems for heat and wave equations: The 1d case," *Inverse Problems and Imaging*, 2014.

[31] L. Bourgeois, "Convergence rates for the quasi-reversibility method to solve the cauchy problem for laplace's equation," *Inverse problems*, vol. 22, no. 2, p. 413, 2006.

[32] L. Bourgeois and J. Dardé, "A duality-based method of quasi-reversibility to solve the cauchy problem in the presence of noisy data," *Inverse Problems*, vol. 26, no. 9, p. 095016, 2010.

[33] C. Clason and M. V. Klibanov, "The quasi-reversibility method for thermoacoustic tomography in a heterogeneous medium," *SIAM Journal on Scientific Computing*, vol. 30, no. 1, pp. 1–23, 2007.

[34] J. Dardé, "Iterated quasi-reversibility method applied to elliptic and parabolic data completion problems," *arXiv preprint arXiv:1503.08641*, 2015.

[35] M. V. Klibanov and F. Santosa, "A computational quasi-reversibility method for cauchy problems for laplaceâs equation," *SIAM Journal on Applied Mathematics*, vol. 51, no. 6, pp. 1653–1675, 1991.

[36] L. H. Nguyen, "An inverse source problem for hyperbolic equations and the lipschitz-like convergence of the quasi-reversibility method," *arXiv preprint arXiv:1806.03921*, 2018.

[37] M. V. Klibanov, "Carleman estimates for the regularization of ill-posed cauchy problems," *Applied Numerical Mathematics*, vol. 94, pp. 46–74, 2015.

[38] L. C. Evans, "Partial differential equations. second. vol. 19," *Graduate Studies in Mathematics. American Mathematical Society, Providence, RI*, 2010.

[39] O. A. Ladyzhenskaya, *The boundary value problems of mathematical physics*, vol. 49. Springer Science & Business Media, 2013.

[40] L. H. Nguyen, Q. Li, and M. V. Klibanov, "A convergent numerical method for a multi-frequency inverse source problem in inhomogenous media," *arXiv preprint arXiv:1901.10047*, 2019.

[41] M. V. Klibanov, J. Li, and W. Zhang, "Convexification for the inversion of a time dependent wave front in a heterogeneous medium," *arXiv preprint arXiv:1812.11281*, 2018.

[42] L. Bourgeois, D. Ponomarev, and J. Dardé, "An inverse obstacle problem for the wave equation in a finite time domain," 2018.

[43] B. Kaltenbacher and W. Rundell, "Regularization of a backwards parabolic equation by fractional operators.," *Inverse Problems & Imaging*, vol. 13, no. 2, 2019.

[44] L. Nguyen, "An inverse space-dependent source problem for hyperbolic equations and the lipschitz-like convergence of the quasi-reversibility method," *Inverse Problems*, 2019.

[45] A. N. Tikhonov, A. Goncharsky, V. Stepanov, and A. G. Yagola, *Numerical methods for the solution of ill-posed problems*, vol. 328. Springer Science & Business Media, 2013.

[46] Nguyen, Hoai-Minh, Nguyen, and L. Hoang, "Cloaking using complementary media for the helmholtz equation and a three spheres inequality for second order elliptic equations," Apr 2015.

[47] M. V. Klibanov, L. H. Nguyen, A. Sullivan, and L. Nguyen, "A globally convergent numerical method for a 1-d inverse medium problem with experimental data," *arXiv preprint arXiv:1602.09092*, 2016.